

Polyakov SU(3) extended linear σ -model: Sixteen mesonic states in chiral phase-structure

Abdel Nasser Tawfik*

Egyptian Center for Theoretical Physics (ECTP),

Modern University for Technology and Information (MTI), 11571 Cairo, Egypt and

World Laboratory for Cosmology And Particle Physics (WLCAPP), Cairo, Egypt

Abdel Magied Diab

World Laboratory for Cosmology And Particle Physics (WLCAPP), Cairo, Egypt

arXiv:1412.2395v1 [hep-ph] 7 Dec 2014

* <http://atawfik.net/>

Abstract

The derivative of the grand potential in the mean field approximation, non-strange and strange condensates and deconfinement phase-transition in thermal and dense hadronic medium are verified in the extended SU(3) linear σ -model (eLSM). In determining the chiral phase-transition, the chiral condensates σ_x and σ_y are analysed. The chiral mesonic phase-structures in temperature- and density-dependence are taken as free parameters to be fitted, experimentally. These parameters are classified corresponding to scalar meson nonets; (pseudo)-scalar and (axial)-vector. For the deconfinement phase-transition, the effective Polyakov loop-potentials ϕ and ϕ^* are utilized. We investigated the in-medium effects on the masses of sixteen mesonic states. The results are presented for two different forms for the effective Polyakov loop-potential and compared with other models with and without anomalous terms. The Polyakov loop potential in (LSM) has considerable effects on the chiral phase-transition in meson masses so that the restoration of the chiral symmetry becomes sharper and faster than LSM. Assuming that the Matsubara frequencies contribute to the meson masses, we normalize all mesonic states with respect to the lowest Matsubara frequency. By doing this, we aim to characterize temperatures and chemical potentials at which the different mesonic bound states dissolve to *free* quarks. It has been found that the various mesonic states have different dissolving temperatures and chemical potentials, i.e. they survive the *typically-averaged* QCD phase boundary, defined by the QCD critical temperatures with varying chemical potentials. The thermal behavior of all meson masses has been investigated in the large- N_c limit and found that the scalar meson masses are T -independent at large N_c and high T (except π and σ). For the pseudoscalar meson masses, the large N_c limit unifies the T -dependence of all states in a universal bundle. The same is also observed for axial and axialvector meson masses in the large- N_c limit.

PACS numbers: 12.39.Fe,12.40.Yx,14.40.-n

Keywords: Chiral Lagrangians, Sigma model, Properties of mesons

Contents	
I. Introduction	3
II. The Extended Linear σ-Model	6
A. Polyakov Loop Potential	9
B. Mean Field Approximation	10
III. Phase Transitions and Their Order Parameters	12
IV. Masses of Sixteen Mesonic States	16
A. Inclusion of Anomalous Terms	16
1. Temperature Dependence	21
2. Density Dependence	26
B. Exclusion of Anomalous Terms	31
1. Temperature Dependence	32
2. Density Dependence	32
C. Numerical Parameters of the Model	34
V. Normalization to the Lowest Matsubara Frequency	35
A. Critical Temperatures and Critical Chemical Potentials	36
VI. Meson masses in large-N_c limit	36
VII. Conclusions	40
Acknowledgements	43
References	43

I. INTRODUCTION

The systematic study of the strongly interacting matter at finite density allows understanding special theories that probably agree with many heavy-ions experiments aiming to tackle the quantum chromodynamic (QCD) phase-transition between the combined nuclear matter and the quark-gluon plasma QGP and improving our understanding of the evolution

of the early Universe. All these can be probed by experiments like STAR at the Relativistic Heavy-Ion Collider RHIC (BNL), ALICE at the Large Hadron Collider LHC (CERN), Compressed Baryon Matter (CBM) at the Facility for Antiproton and Ion Research (GSI) and Baryonic Matter at the Nuclotron (BM@N) at the Nuclotron-based Ion Collider Facility (JINR). The description of the in-medium effects on the thermodynamics quantities is presented in the numerical solutions of difference effective models, especially QCD-like ones. There are two main first-principle models, the Polyakov Nambu-Jona-Lasinio model (PNJL) and Polyakov linear σ model (PLSM) or the Polyakov quark meson model (PQM).

The finite quark masses break explicitly the chiral symmetry of QCD. In this case, one has to resort numerical calculations in order to determine the order of the chiral phase-transition, such as $SU(3)_r \times SU(3)_\ell$ linear σ -model [1]. The description of all mesonic states is possible through $\langle \bar{q}q \rangle = \langle \bar{q}_r q_\ell + \bar{q}_\ell q_r \rangle \neq 0$ [2], where the quark constituents of the scalar mesons were debated, many decades ago [3, 4]. The chiral structure of four categories of mesonic states is classified through the quantum numbers, the orbital angular momentum J , parity P and charge conjugate C , which can be constructed from u - and d - and s -quarks, into scalars ($J^{PC} = 0^{++}$) and pseudoscalars ($J^{PC} = 0^{-+}$), vectors ($J^{PC} = 1^-$) and axial-vectors ($J^{PC} = 1^{++}$). As the chiral symmetry is explicitly broken, the deconfinement phase-transition would affect the mass spectrum and show under which conditions certain state degenerates with another one and when the thermal and dense evolution goes through phase transition. The in-medium masses of the some different mesonic states are analysed, systematically. We study the effects of finite temperature of sixteen mesonic states at vanishing and finite baryon-chemical potentials and also the density-dependence of the same states at finite temperatures. Thus, the extension of LSM to PLSM, in which information about the confining gluonic sector is embedded in form of the Polyakov-loop potential is very crucial. The Polyakov loop-potential is extracted from pure Yang-Mills lattice simulations [5–8]. The LSM at finite temperature was implemented to investigate the chiral phase-transition [9, 10]. The $U(N_f)_r \times U(N_f)_l$ LSM with $N_f = 2, 3$ or even 4 quark flavors was also applied [11–14].

In LSM, the thermodynamic properties like pressure, equation of state, square of the speed of sound, specific heat and trace anomaly [15–18] can be evaluated at finite and vanishing baryon chemical potential. Furthermore, the normalized and non-normalized higher order moments of the particle multiplicity have been analysed [18–20]. Also, the chiral phase-structure of the scalar and pseudoscalar mesonic states at finite and vanishing temperatures

were evaluated [21] with and without the presence of axial anomaly and with the inclusion of the Polyakov loop correction [22, 23]. At finite isospin chemical potential, a three-flavor NJL model for scalar and pseudoscalar mesonic states was presented [24]. In a three-flavor PNJL model [25] it was discussed how the inclusion of the Polyakov loop-potential in the NJL model affects the results of the meson masses. Results of $2 + 1$ flavor lattice QCD of pseudoscalar and vector meson states was presented [26, 27]. The results deduced from Hot QCD [26] and PACS-CS [27] are compared with the Particle Data Group (PDG) [28]. An excellent agreement was reported [21–24, 26–28].

In general, the PLSM has a wide range of implications. Not only the thermodynamics quantities [16, 18, 29, 30] but it can also describe the higher order moments of the particle multiplicity [18, 19], the hadron vacuum phenomenology [31–36] and estimates the effects of the chiral and deconfinement phase-transitions [37–39] besides the chiral phase-structure of hadrons (the spectrum of hadrons in both thermal- and hadronic dense-medium) [21–23, 40, 41], the decay width and the scattering length of hadronic states [31, 33, 35, 36, 42, 43].

In the present work, we introduce a systematic study using the chiral symmetric linear σ -model. We included in it scalar, pseudoscalar, vector, and axial-vector fields and estimate the representation of all these four categories in dependence on the temperature T and the baryon chemical potential μ . This allows to define the characteristics of the chiral phase-structure for all these mesonic states, i.e., in thermal and hadronic dense medium and determine the critical temperature and density at which each mesonic state breaks into its free quarks.

The arrangement of this paper is organized as follows. Section II gives details about the extended linear σ -model eLSM, where the Lagrangian of the scalar and pseudoscalar fields are extended to include vector and axial-vector fields as well and interaction between mesonic sector in the presence of $U(1)_A$ symmetry breaking. The Polyakov loop-correction to the Lagrangian of eLSM is introduced in section II A. The mean field approximation is outlined in Sec. II B. The phase transition including quark condensates and order parameters shall be estimated in Sec. III. Topics like deconfinement (crossover) phase-transition and order parameter due to chiral symmetry breaking shall be studied as well. In section IV, we introduce the Polyakov loop-potential to LSM (hereafter called PLSM) and investigate sixteen mesonic states in thermal (Sec. IV A 1) and hadronic dense medium (Sec. IV A 2). The critical temperature and the baryon chemical potential, at which each bound hadron state should dissolve into free quarks (QGP) shall be introduced in Sec. V. Section VII is

devoted to the conclusions.

II. THE EXTENDED LINEAR σ -MODEL

The Lagrangian of LSM with $N_f = 3$ quark flavors and $N_c = 3$ color degrees of freedom, where the quarks couple to the Polyakov loop-dynamics Φ -field represents a complex (3×3) -matrix for the $SU(3)_L \times SU(3)_R$ symmetric LSM Lagrangian $\mathcal{L}_{chiral} = \mathcal{L}_q + \mathcal{L}_m$, where the fermionic part reads

$$\mathcal{L}_q = \bar{q} [i\partial - g T_a (\sigma_a + i\gamma_5 \pi_a + \gamma_\mu V_a^\mu + \gamma_\mu \gamma_5 A_a^\mu)] q, \quad (1)$$

where the μ is an additional Lorentz index [69], g is the flavor-blind Yukawa coupling of the quarks to the mesonic contribution $\mathcal{L}_m = \mathcal{L}_{SP} + \mathcal{L}_{VA} + \mathcal{L}_{Int} + \mathcal{L}_{U(1)_A}$ represented to \mathcal{L}_{SP} scalars ($J^{PC} = 0^{++}$) and pseudoscalars ($J^{PC} = 0^{-+}$), \mathcal{L}_{VA} to vectors ($J^{PC} = 1^-$) and axial-vectors ($J^{PC} = 1^{+-}$) mesons and \mathcal{L}_{Int} being the interaction between them. Finally the Lagrangian of the anomaly term is given by $\mathcal{L}_{U(1)_A}$ [1, 43–47].

$$\mathcal{L}_{SP} = \text{Tr}(\partial_\mu \Phi^\dagger \partial^\mu \Phi - m^2 \Phi^\dagger \Phi) - \lambda_1 [\text{Tr}(\Phi^\dagger \Phi)]^2 - \lambda_2 \text{Tr}(\Phi^\dagger \Phi)^2 + \text{Tr}[H(\Phi + \Phi^\dagger)], \quad (2)$$

$$\begin{aligned} \mathcal{L}_{AV} = & -\frac{1}{4} \text{Tr}(L_{\mu\nu}^2 + R_{\mu\nu}^2) + \text{Tr} \left[\left(\frac{m_1^2}{2} + \Delta \right) (L_\mu^2 + R_\mu^2) \right] \\ & + i\frac{g_2}{2} (\text{Tr}\{L_{\mu\nu}[L^\mu, L^\nu]\} + \text{Tr}\{R_{\mu\nu}[R^\mu, R^\nu]\}) \\ & + g_3 [\text{Tr}(L_\mu L_\nu L^\mu L^\nu) + \text{Tr}(R_\mu R_\nu R^\mu R^\nu)] + g_4 [\text{Tr}(L_\mu L^\mu L_\nu L^\nu) + \text{Tr}(R_\mu R^\mu R_\nu R^\nu)] \\ & + g_5 \text{Tr}(L_\mu L^\mu) \text{Tr}(R_\nu R^\nu) + g_6 [\text{Tr}(L_\mu L^\mu) \text{Tr}(L_\nu L^\nu) + \text{Tr}(R_\mu R^\mu) \text{Tr}(R_\nu R^\nu)], \end{aligned} \quad (3)$$

$$\mathcal{L}_{Int} = \frac{h_1}{2} \text{Tr}(\Phi^\dagger \Phi) \text{Tr}(L_\mu^2 + R_\mu^2) + h_2 \text{Tr}[|L_\mu \Phi|^2 + |\Phi R_\mu|^2] + 2h_3 \text{Tr}(L_\mu \Phi R^\mu \Phi^\dagger), \quad (4)$$

$$\mathcal{L}_{U(1)_A} = c[\text{Det}(\Phi) + \text{Det}(\Phi^\dagger)] + c_0[\text{Det}(\Phi) - \text{Det}(\Phi^\dagger)]^2 + c_1[\text{Det}(\Phi) + \text{Det}(\Phi^\dagger)] \text{Tr}[\Phi \Phi^\dagger]. \quad (5)$$

The first Lagrangian, Eq. (2), represents to kinetic and potential terms for the scalar meson nonets. The third term stands for the explicit symmetry breaking defined in Eq. (10). This Lagrangian creates scalar and pseudoscalar mesonic states defined in Φ nonets, Eq. (9). While the second Lagrangian, Eq. (3), represents the vector meson nonets involving explicit symmetry breaking in the second term defined Eq. (10). The 3×3 matrix of the vector meson nonets involves vector and axial-vector fields, Eq. (9). This creates the vector and axial-vector mesonic states and the interactions between the (pseudo)-scalar and (axial)-vector introduced in Eq. (4). As the symmetry is broken, explicitly and spontaneously, the anomaly term $\mathcal{L}_{U(1)_A}$ in $(SU(3)_r \times SU(3)_\ell)$ should be introduced into the effective Lagrangian

and c, c_0, c_1 are the parameters to be determined, experimentally [33]. The first two terms approximate the original axial anomaly term [48, 49], while the third term is a mixed one. It is proportionally to the first term. The concept of choosing the first anomaly term is essential, in which the other terms are used to compare with other effects of the different anomaly terms on the hadronic structure [47].

To describe experimental data, terms of large order in order should be included in the LSM with local chiral symmetry [33]. The $\mathcal{L}_{U(1)_A}$ symmetry of the classical QCD Lagrangian is anomalous [50] also known as the QCD vacuum anomaly [21, 50], i.e., broken by quantum effects. Without anomaly a ninth pseudoscalar Goldstone boson corresponding to the spontaneous breaking of the chiral $U(3)_\ell \times U(3)_r$ symmetry should unfold [21, 50]. Because the hadronic theory is apparently not fundamental and supposed to be valid for mass scale of 1 – 2 GeV [33], the local chiral symmetry would not cause big problem. Nevertheless, the constraint-terms are conjectured to affect such QCD approaches [33]. This well-known $\mathcal{L}_{U(1)_A}$ problem of QCD is effectively controlled by the anomaly term c of the Lagrangian [51]. The squared tree-level masses of mesons m^2 and m_1^2 contain a contribution arising from the spontaneous symmetry breaking [33].

The introduction of scalar and vector meson nonets into the Lagrangian of eLSM requires a definition for the contra-covariant derivative of the quark meson contribution represented in Eq. (6), where the degrees of freedom of the scalar Φ and vector L^μ and R^μ meson nonets are coupling as well to the electromagnetic field A^μ . Eqs. (7) and (8) are the left-handed and right-handed field strength tensors, respectively. they represent the self interaction between the vector and axial-vector mesons with the electromagnetic field A^μ . The local chiral invariance emerging from the globally invariant eLSM Lagrangian requires that $g_1 = g_2 = g_3 = g_4 = g_5 = g_6 = g$ [33]

$$D^\mu \Phi \equiv \partial^\mu \Phi - ig_1(L^\mu \Phi - \Phi R^\mu) - ieA^\mu [T_3, \Phi], \quad (6)$$

$$L^{\mu\nu} \equiv \partial^\mu L^\nu - ieA^\mu [T_3, L^\nu] - \{\partial^\nu L^\mu - ieA^\nu [T_3, L^\mu]\}, \quad (7)$$

$$R^{\mu\nu} \equiv \partial^\mu R^\nu - ieA^\mu [T_3, R^\nu] - \{\partial^\nu R^\mu - ieA^\nu [T_3, R^\mu]\}. \quad (8)$$

It is apparent that $T_a = \hat{\lambda}_a/2$ with $a = 0 \dots 8$ are nine $U(3)$ generators, where $\hat{\lambda}_a$ are the Gell-Mann matrices with the fields Φ of 3×3 complex matrix comprising of the scalars σ_a ($J^{PC} = 0^{++}$), pseudoscalars π_a ($J^{PC} = 0^{-+}$), V_a^μ , vectors ($J^{PC} = 1^-$) and A_a^μ axial-vectors

($J^{PC} = 1^{++}$) mesonic states given by

$$\begin{aligned}\Phi &= \sum_{a=0}^8 T_a (\sigma_a + i\pi_a), \\ L^\mu &= \sum_{a=0}^8 T_a (V_a^\mu + A_a^\mu), \\ R^\mu &= \sum_{a=0}^8 T_a (V_a^\mu - A_a^\mu).\end{aligned}\tag{9}$$

$\lambda_0 = \sqrt{\frac{2}{3}} \mathbf{1}$ and T_a are normalized such that they obey the $U(3)$ algebra [52]. The chiral symmetry is explicitly broken by

$$H = \sum_{a=0}^8 T_a h_a \quad , \quad \Delta = \sum_{a=0}^8 T_a \delta_a.\tag{10}$$

The symmetry breaking terms are originated by $U(3)_L \times U(3)_R = U(3)_V \times U(3)_A$. The terms are proportional to the matrix H and Δ as given in Eq. (10). This relation describes the explicit symmetry breaking due to

- finite quark masses in the (pseudo)-scalar and (axial)-vector sectors,
- breaking $U(3)_A$ if $H_0, \Delta_0 \neq 0$,
- Breaking $U(3)_V \rightarrow SU(2)_V \times U(1)_V$ if $H_8, \Delta_8 \neq 0$.

For more details, the readers are referred to Ref. [41]. We take into consideration that of the spontaneous chiral symmetry breaking takes part in vacuum state. Then a finite vacuum expectation value of the fields Φ and $\bar{\Phi}$ are conjectured to carry the quantum numbers of the vacuum [?]. As a result, the components of the explicit symmetry breaking term in diagonal are h_0, h_3 and h_8 and δ_0, δ_3 and δ_8 should not vanish [?]. This leads to exacting three finite condensates $\bar{\sigma}_0, \bar{\sigma}_3$ and $\bar{\sigma}_8$. On the other hand, $\bar{\sigma}_3$ breaks the isospin symmetry $SU(2)$ [?]. To avoid this situation, we restrict ourselves to $SU(3)$. This can be $N_f = 2 + 1$ [21] flavor symmetry breaking pattern. Correspondingly, two degenerate light (u-quark and d-quark) and one heavier quark flavor (s-quark), i.e., $m_u = m_d \neq m_s$ are assumed. Furthermore, the violation of the isospin symmetry is neglected. This facilitates the choice of h_a ($h_0 \neq 0, h_3 = 0$ and $h_8 \neq 0$) and for δ_a ($\delta_0 \neq 0, \delta_3 = 0$ and $\delta_8 \neq 0$).

$$T_a \sigma_a = \frac{1}{\sqrt{2}} \begin{pmatrix} \frac{1}{\sqrt{2}} a_0^0 + \frac{1}{\sqrt{6}} \sigma_8 + \frac{1}{\sqrt{3}} \sigma_0 & a_0^- & \kappa^- \\ a_0^+ & -\frac{1}{\sqrt{2}} a_0^0 + \frac{1}{\sqrt{6}} \sigma_8 + \frac{1}{\sqrt{3}} \sigma_0 & \bar{\kappa}^0 \\ \kappa^+ & \kappa^0 & -\frac{2}{\sqrt{3}} \sigma_8 + \frac{1}{\sqrt{3}} \sigma_0 \end{pmatrix}, \quad (11)$$

$$T_a \pi_a = \frac{1}{\sqrt{2}} \begin{pmatrix} \frac{1}{\sqrt{2}} \pi^0 + \frac{1}{\sqrt{6}} \pi_8 + \frac{1}{\sqrt{3}} \pi_0 & \pi^- & K^- \\ \pi^+ & -\frac{1}{\sqrt{2}} \pi^0 + \frac{1}{\sqrt{6}} \pi_8 + \frac{1}{\sqrt{3}} \pi_0 & \bar{K}^0 \\ K^+ & K^0 & -\frac{2}{\sqrt{3}} \pi_8 + \frac{1}{\sqrt{3}} \pi_0 \end{pmatrix}. \quad (12)$$

and

$$T_a V_a^\mu = \frac{1}{\sqrt{2}} \begin{pmatrix} \frac{\omega_0 + \rho^0}{\sqrt{2}} & \rho^+ & K^{*+} \\ \rho^- & \frac{\omega_0 - \rho^0}{\sqrt{2}} & K^{*0} \\ K^{*-} & \bar{K}^{*0} & \omega_8 \end{pmatrix}^\mu, \quad (13)$$

$$T_a A_a^\mu = \frac{1}{\sqrt{2}} \begin{pmatrix} \frac{f_{10} + a_1^0}{\sqrt{2}} & a_1^+ & K_1^+ \\ a_1^- & \frac{f_{10} - a_1^0}{\sqrt{2}} & K_1^0 \\ K_1^- & \bar{K}_1^0 & f_{18} \end{pmatrix}^\mu. \quad (14)$$

It would be more convenient when converting the condensates σ_0 and σ_8 into a pure non-strange σ_x and pure strange σ_y quark flavor [53]

$$\begin{pmatrix} \sigma_x \\ \sigma_y \end{pmatrix} = \frac{1}{\sqrt{3}} \begin{pmatrix} \sqrt{2} & 1 \\ 1 & -\sqrt{2} \end{pmatrix} \begin{pmatrix} \sigma_0 \\ \sigma_8 \end{pmatrix}. \quad (15)$$

It is worthwhile to mention that $\sigma \ni (\sigma_a, \pi_a, V_a^\mu, A_a^\mu)$.

A. Polyakov Loop Potential

The Lagrangian of LSM can be coupled to the Polyakov loop-dynamics [16, 21],

$$\mathcal{L} = \mathcal{L}_{chiral} - \mathcal{U}(\phi, \phi^*, T), \quad (16)$$

The second term in Eq. (16), $\mathcal{U}(\phi, \phi^*, T)$, represents the effective Polyakov loop-potential [5], which gives the dynamics of the thermal expectation value of a color traced Wilson loop in the temporal direction [5]

$$\phi(\vec{x}) = \frac{1}{N_c} \langle \mathcal{P}(\vec{x}) \rangle. \quad (17)$$

Then, the Polyakov-loop potential and its conjugate read

$$\phi = \langle \text{Tr}_c \mathcal{P} \rangle / N_c, \quad (18)$$

$$\phi^* = \langle \text{Tr}_c \mathcal{P}^\dagger \rangle / N_c, \quad (19)$$

where \mathcal{P} is the Polyakov loop, which can be expressed as a matrix in the color space [5]

$$\mathcal{P}(\vec{x}) = \mathcal{P} \exp \left[i \int_0^\beta d\tau A_0(\vec{x}, \tau) \right], \quad (20)$$

where $\beta = 1/T$ is the inverse temperature and A_0 is the temporal component of Euclidean vector field [5, 6]. The Polyakov loop matrix can be re-expressed as a diagonal representation [54] as shown in Eqs. (18) and (19) where the gauge field $A_\mu = g_s A_\mu^a \lambda^a / 2$ with $a = 1, \dots, N_c^2 - 1$ and the gauge coupling g_s . The coupling between the Polyakov loop and the quarks is unrivalled and given by the covariant derivative $D_\mu = \partial_\mu - i A_\mu$, Eq. (16), where $A_\mu = \delta_{\mu 0} A_0$ is given in the chiral limit, Eq. (16) and therefore is invariant under the chiral flavor group. This is the same as the original QCD Lagrangian [55–57]. In order to reproduce the thermodynamic behavior of the Polyakov loop for pure gauge case, we use temperature-dependent potential $U(\phi, \phi^*, T)$. This should agree with lattice QCD data and have $Z(3)$ center symmetry [55–58] as that of the pure gauge QCD Lagrangian [55, 58]. In case of no quarks, then $\phi = \phi^*$ and the Polyakov loop is considered as an order parameter for the deconfinement phase-transition [55, 58]. In the present work, we use $U(\phi, \phi^*, T)$ as a polynomial expansion in ϕ and ϕ^* [55–58]

$$\frac{\mathcal{U}(\phi, \phi^*, T)}{T^4} = -\frac{b_2(T)}{2} |\phi|^2 - \frac{b_3}{6} (\phi^3 + \phi^{*3}) + \frac{b_4}{4} (|\phi|^2)^2, \quad (21)$$

where

$$b_2(T) = a_0 + a_1 \left(\frac{T_0}{T} \right) + a_2 \left(\frac{T_0}{T} \right)^2 + a_3 \left(\frac{T_0}{T} \right)^3. \quad (22)$$

In order to reproduce pure gauge QCD thermodynamics and the behavior of the Polyakov loop as a function of temperature, we use the parameters listed out in Tab. I. For a much better agreement with the lattice QCD results, the deconfinement temperature T_0 in the pure gauge sector is fixed at 270 MeV.

B. Mean Field Approximation

The change of particle and antiparticle number is governed by the grand canonical partition function. To construct the partition function, we take into consideration a spatially

$a_0 = 6.75,$	$a_1 = -1.95,$	$a_2 = 2.625,$	$a_3 = -7.44$
$b_3 = 0.75$		$b_4 = 7.5$	

Tab. I: The potential parameters are adjusted to the pure gauge lattice data such that the equation of state and the Polyakov loop expectation values are reproduced [55].

uniform system in a thermal equilibrium at finite temperature T and quark chemical potential μ_f , where f stands for u, d and s quarks. A path integral over the quark, antiquark and meson fields leads to [21]

$$\begin{aligned} \mathcal{Z} &= \text{Tr} \exp[-(\hat{\mathcal{H}} - \sum_{f=u,d,s} \mu_f \hat{\mathcal{N}}_f)/T] \\ &= \int \prod_a \mathcal{D}\sigma_a \mathcal{D}\pi_a \int \mathcal{D}\psi \mathcal{D}\bar{\psi} \exp \left[\int_x (\mathcal{L} + \sum_{f=u,d,s} \mu_f \bar{\psi}_f \gamma^0 \psi_f) \right], \end{aligned} \quad (23)$$

where $\int_x \equiv i \int_0^{1/T} dt \int_V d^3x$ and V is the volume of the system. For a symmetric quark matter, the uniform blind chemical potential fulfils the conditions that $\mu_f \equiv \mu_u = \mu_d = \mu_s$ [21, 59, 61]. In the action, we replace the meson fields by their expectation values $\bar{\sigma}_x$ and $\bar{\sigma}_y$ [62]. To estimate the integration over the fermions yields, other methods have been introduced [62]. The effective mesonic potential can be deduced. The thermodynamic potential density reads

$$\Omega(T, \mu) = \frac{-T \ln \mathcal{Z}}{V} = U(\sigma_x, \sigma_y) + \mathcal{U}(\phi, \phi^*, T) + \Omega_{\bar{q}q}(T, \mu_f). \quad (24)$$

The explicit quark contribution to LSM is given as

$$\Omega_{\bar{q}q}(T, \mu_f) = \nu_c T \sum_{f=u,d,s} \int_0^\infty \frac{d^3k}{(2\pi)^3} \{ \ln(1 - n_{q,f}(T, \mu_f)) + \ln(1 - n_{\bar{q},f}(T, \mu_f)) \}, \quad (25)$$

with the usual fermionic occupation numbers (for quarks)

$$n_{q,f}(T, \mu_f) = \frac{1}{1 + \exp[(E_f - \mu_f)/T]}. \quad (26)$$

For antiquarks $n_{\bar{q},f}(T, \mu_f) \equiv n_{q,f}(T, -\mu_f)$. The number of internal quark degrees of freedom is denoted by $\nu_c = 2N_c = 6$. The flavor-dependent single-particle energies are

$$E_f = \sqrt{k^2 + m_f^2}, \quad (27)$$

where m_f is the flavor-dependent quark masses. Also, the light quark sector is conjectured to decouple from strange quark sector [53]. Assuming degenerate light quarks, i.e., $l \equiv u, d$, then, the masses can be simplified as [53]

$$m_l = g \frac{\sigma_x}{2}, \quad (28)$$

$$m_s = g \frac{\sigma_y}{\sqrt{2}}. \quad (29)$$

And for PLSM, the quarks and antiquarks contributions to the potential are given as [62]

$$\begin{aligned} \Omega_{\bar{q}q}(T, \mu) = & -\nu_c T \sum_{f=l,s} \int_0^\infty \frac{d^3\vec{p}}{(2\pi)^3} \left\{ \ln [1 + 3(\phi + \phi^* e^{-(E_f - \mu)/T}) \times e^{-(E_f - \mu)/T} + e^{-3(E_f - \mu)/T}] \right. \\ & \left. + \ln [1 + 3(\phi^* + \phi e^{-(E_f + \mu)/T}) \times e^{-(E_f + \mu)/T} + e^{-3(E_f + \mu)/T}] \right\}, \quad (30) \end{aligned}$$

Based on non-strange σ_x and strange σ_y condensates and taking into consideration Eq. (15), the purely mesonic potential reads

$$\begin{aligned} U(\sigma_x, \sigma_y) = & -h_x \sigma_x - h_y \sigma_y + \frac{m^2}{2} (\sigma_x^2 + \sigma_y^2) - \frac{c}{2\sqrt{2}} \sigma_x^2 \sigma_y + \frac{\lambda_1}{2} \sigma_x^2 \sigma_y^2 \\ & + \frac{1}{8} (2\lambda_1 + \lambda_2) \sigma_x^4 + \frac{1}{4} (\lambda_1 + \lambda_2) \sigma_y^4. \quad (31) \end{aligned}$$

III. PHASE TRANSITIONS AND THEIR ORDER PARAMETERS

By minimizing the thermodynamic potential, Eq. (24), with respect to σ_x , σ_y , ϕ and ϕ^* , we obtain a set of four equations of motion σ_x , σ_y , ϕ and ϕ^* .

$$\frac{\partial \Omega}{\partial \sigma_x} = \frac{\partial \Omega}{\partial \sigma_y} = \frac{\partial \Omega}{\partial \phi} = \frac{\partial \Omega}{\partial \phi^*} \Big|_{\sigma_x = \bar{\sigma}_x, \sigma_y = \bar{\sigma}_y, \phi = \bar{\phi}, \phi^* = \bar{\phi}^*} = 0, \quad (32)$$

meaning that $\sigma_x = \bar{\sigma}_x$, $\sigma_y = \bar{\sigma}_y$, $\phi = \bar{\phi}$ and $\phi^* = \bar{\phi}^*$ being the global minimum, where all thermodynamics quantities are related to the parameters σ_x , σ_y , ϕ and ϕ^* .

In determining the chiral phase-transition, σ_x and σ_y , and in determining the deconfinement phase-transition, ϕ and ϕ^* should be estimated. The chiral mesonic phase-structures in temperature- and density-dependence are taken as free parameters to be fitted, experimentally. These parameters are classified corresponding to scalar meson nonets m^2 , h_x , h_y , λ_1 , λ_2 and c [21]. The vector meson nonets have the parameters m_1^2 , g_1 , h_1 , h_2 , h_3 , δ_x and δ_y [31]. In the present paper, we mainly use $\sigma = 800$ MeV.

At vanishing temperature, the chiral condensates for light and strange quarks are taken as $\sigma_{x_0} = 92.4$ MeV and $\sigma_{y_0} = 94.5$ MeV, respectively [16, 21]. These values are used to

normalize their thermal evolution at vanishing chemical potential. In this limit, the two Polyakov loops are identical, i.e. $\langle\phi\rangle = \langle\phi^*\rangle$. To determining the critical temperature of the phase transition (crossover), two approaches can be implemented:

- The first one is the point, at which the order parameter intersects with the curve of the corresponding chiral condensate.
- The second one is based on the peak in the temperature derivative of the condensates or the chiral susceptibilities for strange and nonstrange quarks. The peak should be ordered to the critical temperature.

The first approach was used to derive the results depicted in Fig. 1. Accordingly, we find that the chiral restoration of the non-strange condensate is related to $T_c^q \sim 181$ MeV, while for the strange quark to $T_c^s \sim 270$ MeV.

The lattice QCD simulations prefer dimensionless quantities. Therefore, the chiral order parameter is expressed in the chiral condensate [63]

$$M_b = \frac{m_s \langle \bar{\sigma}_x(T, \mu) \rangle}{T^4}. \quad (33)$$

The right-hand panel of Fig. 1 compares the chiral condensate from HISQ/tree with temporal dimensions $N_t = 8$, and two quark masses $M_q/M_s = 0.025$ and $M_q/M_s = 0.05$ in $\mathcal{O}(4)$ lattices [63] with PLSM calculations for M_b .

Using for light constituent quark mass the value $m_l = 300$ MeV, we obtain $g = 6.5$ and predict that the strange constituent quark mass reads $m_s \sim 433$ MeV. These are normalized to values at zero temperature T at vanishing baryon chemical potential μ . In cases of finite T at vanishing μ and vanishing T and finite μ , the chiral phase-transition is determined by non-strange and strange quarks fields, Eqs. (28) and (29) as shown in Fig. 2. The left-hand panel of Fig. 2 shows the thermal evolution of non-strange and strange quarks at vanishing μ . The right-hand panel shows their density dependence at $T = 10$ MeV. The contribution of finite quark mass requires the estimation of the chiral phase-transition. To this end, the normalized condensates are studied in T - and μ -dependence till they vanish.

For the in-medium thermal and dense effects on the mesonic masses, we present in the left-hand panel of Fig. 3 the chiral condensates at varying temperatures and fixed baryon chemical potentials. In doing this, we take into consideration the thermal and dense dependences of the chiral condensates. For instance, we present the chiral condensates at different temperatures and chemical potentials. At these temperatures and chemical potentials, we

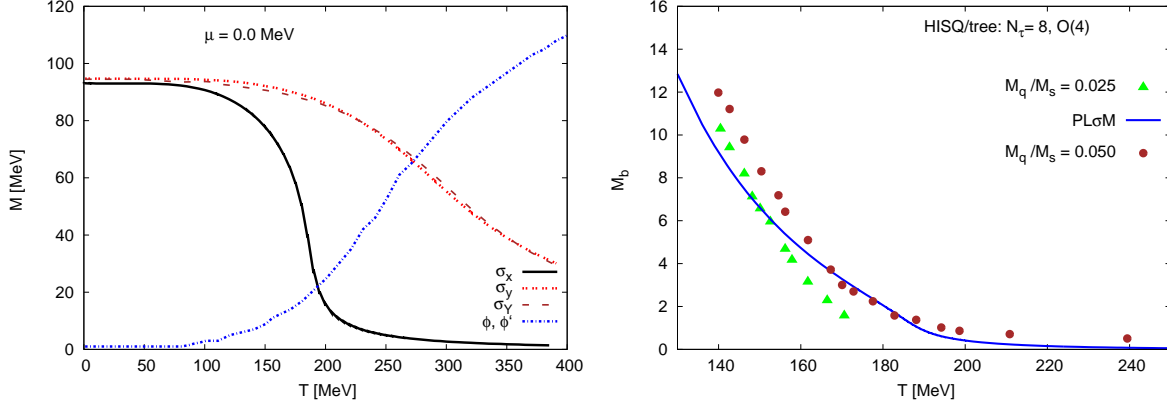


Fig. 1: (color online) Left-hand panel: the chiral condensates σ_x and σ_y (solid and dotted curves, respectively) and the Polyakov loops ϕ and ϕ^* (dashed curve at $c = 0$, i.e. without anomaly) are given as functions of the temperature at vanishing baryon chemical potential. At $\mu = 0$ MeV, the two Polyakov loops are identical, i.e. $\phi = \phi^*$. Right-hand panel: the chiral condensate in $O(4)$ lattices [63] with HISQ/tree with $N_t = 8$ is compared with the PLSM calculations (solid curve). The rectangular symbols stand for $M_q/M_s = 0.025$ and the circular ones represent $M_q/M_s = 0.05$.

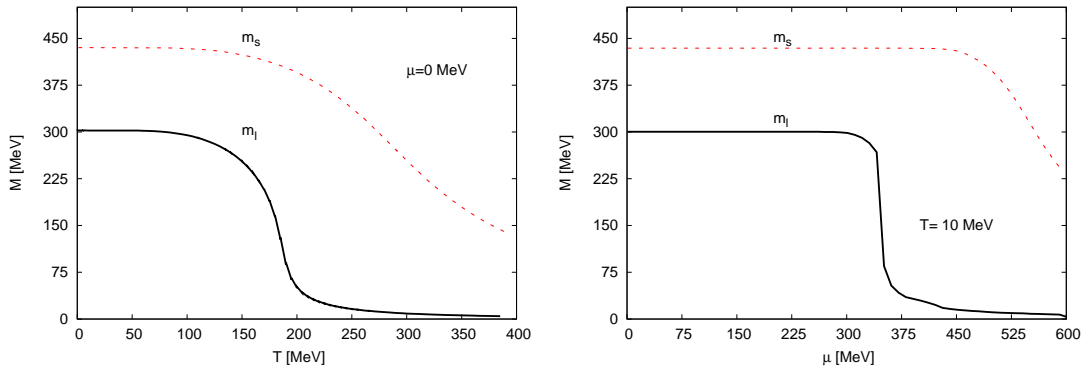


Fig. 2: (color online) The left-hand panel presents the thermal evolution of non-strange m_l (solid curve) and strange (dashed curve) at $\mu = 0$ MeV. The right-hand panel shows their dependence on the baryon chemical potential at a fixed temperature $T = 10$ MeV.

should estimate the thermal and dense dependences of the mesonic states. We notice that the values of σ_x and σ_y decrease with increasing T . There is a rapid decrease within a narrow range of temperatures. The light quarks are more sensitive than the strange quarks. This likely characterizes the chiral phase-transition.

There is a similar decrease in both quantities with increasing hadronic dense medium (baryon chemical potential), right-hand panel of Fig. 3. We notice that the sudden decrease around the chiral phase-transition is sharper than the one in the left-hand panel. This would

indicate that the chiral phase-transition at large density and low temperature (very near to the abscissa of the QCD phase diagram [64]) is much prompt than the one at low chemical potential and high temperature. The earlier would likely be characterized as a first order phase-transition, while the latter one as a moderate phase-transition (crossover).

We also notice that the fast decrease of σ_x takes place earlier and faster than that of σ_y . For instance, in the left-hand panel of fig. 2, we find that $T_c^q = 181$ MeV at vanishing density, and the decreases are smooth, while at finite baryon chemical density and fixed $T = 10$ MeV, the critical value $\mu = 360$ MeV. This would be interpreted as a *smooth* phase-transition know as crossover [65]. Thus, in presence of the Polyakov loop-potential, $UA(1)$ of the symmetry breaking term is kept constant throughout the chiral and deconfinement phase-transition.

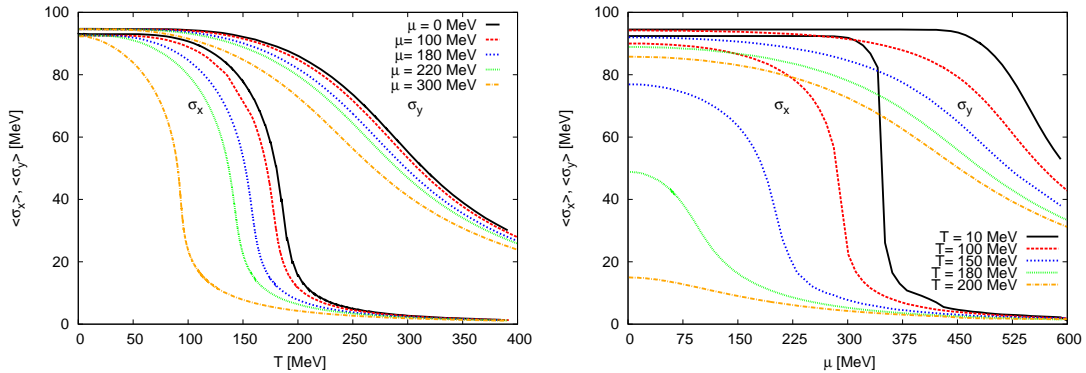


Fig. 3: (Color online) Left-hand panel: the averaged chiral condensate, $\langle \sigma_x \rangle$, is given as functions of temperature at different chemical potentials, $\mu = 0, 100, 180, 200$ and 300 MeV (solid curves from on top, then downwards to bottom, respectively). For the chiral condensate $\langle \sigma_y \rangle$, we fix the same values of μ . The right-hand panel presents the dependence on μ , where the temperatures are fixed at the given values $T = 10, 100, 150, 180$ and 200 MeV (solid curves from on top, then downwards to bottom, respectively).

For the results depicted in Fig. 4, we analyse the deconfinement phase-transition at varying baryon chemical potentials and temperatures and include the Ploykov loop corrections to the mesonic masses at fixed five different temperatures and five different chemical potentials. The thermal effects of the hadronic medium on the evolution of ϕ seems to be very smooth. In hadronic dense medium, the slope of $\phi(\mu)$ seems to depend on the temperature. It is always positive and increases rapidly with μ , while $\phi(\mu)^*$ decreases slowly comparing to $\phi(\mu)$. Both quantities intersect at a characteristic value of μ depending on value of the

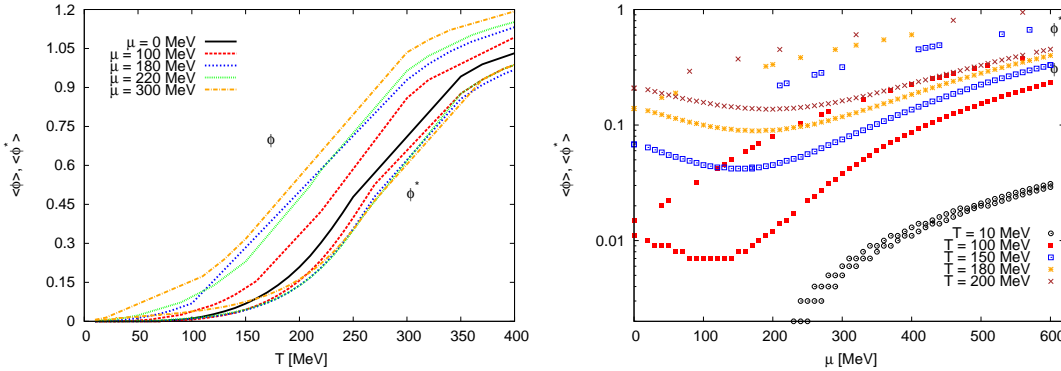


Fig. 4: (Color online) The expectation values Polyakov loop, ϕ and ϕ^* , (left-hand panel) are given as functions of temperature at different chemical potentials, $\mu = 0, 100, 180, 200$ and 300 MeV for ϕ^* (solid curve, from the forward to backwards, respectively) and for ϕ (solid curve, from the backward to forward, respectively). The chiral condensates, ϕ and ϕ^* , (right-hand panel) are given as functions of the chemical potential numerically in log-scale at different temperatures $T = 10, 100, 150, 180$ and 200 MeV as points (from backward to forward, respectively) ϕ (top curves) and ϕ^* (bottom curves).

temperature T .

IV. MASSES OF SIXTEEN MESONIC STATES

A. Inclusion of Anomalous Terms

It is assumed that the contribution of the quark potential to the Lagrangian vanishes in the vacuum. Therefore, only the mesonic part of the potential determines the mass matrix, entirely. In other words, the meson masses do not receive any contribution from quark/antiquark in vacuum and thus the meson masses are governed only by mesonic potential [21, 41]. The masses are defined by the second derivative with respect to the corresponding fields of the grand potential $\Omega(T, \mu_f)$, Eq. (24), evaluated at its minimum Eq. (34). In our case, the minimum is estimated by vanishing expectation values of all scalar, pseudoscalar, vector and axial-vector fields. Only two of the pure strange $\bar{\sigma}_x$ and non-strange $\bar{\sigma}_y$ condensates are finite

$$m_{i,ab}^2 = \left. \frac{\partial^2 \Omega(T, \mu_f)}{\partial \zeta_{i,a} \partial \zeta_{i,b}} \right|_{\min}, \quad (34)$$

where i stands for scalar, pseudoscalar, vector and axial-vector mesons and a and b range from $0, \dots, 8$. In vacuum, the mesonic sectors are formulated in the non-strange and strange

basis:

- Scalar mesonic states

The squared masses for scalar sector ($i = s$) are given as

$$m_{a_0}^2 = m^2 + \lambda_1 (\bar{\sigma}_x^2 + \bar{\sigma}_y^2) + \frac{3\lambda_2}{2} \bar{\sigma}_x^2 + \frac{\sqrt{2}c}{2} \bar{\sigma}_y, \quad (35)$$

$$m_{\kappa}^2 = m^2 + \lambda_1 (\bar{\sigma}_x^2 + \bar{\sigma}_y^2) + \frac{\lambda_2}{2} (\bar{\sigma}_x^2 + \sqrt{2}\bar{\sigma}_x\bar{\sigma}_y + 2\bar{\sigma}_y^2) + \frac{c}{2} \bar{\sigma}_x, \quad (36)$$

$$m_{\sigma}^2 = m_{s,00}^2 \cos^2 \theta_s + m_{s,88}^2 \sin^2 \theta_s + 2m_{s,08}^2 \sin \theta_s \cos \theta_s, \quad (37)$$

$$m_{f_0}^2 = m_{s,00}^2 \sin^2 \theta_s + m_{s,88}^2 \cos^2 \theta_s - 2m_{s,08}^2 \sin \theta_s \cos \theta_s, \quad (38)$$

with

$$m_{s,00}^2 = m^2 + \frac{\lambda_1}{3} (7\bar{\sigma}_x^2 + 4\sqrt{2}\bar{\sigma}_x\bar{\sigma}_y + 5\bar{\sigma}_y^2) + \lambda_2 (\bar{\sigma}_x^2 + \bar{\sigma}_y^2) - \frac{\sqrt{2}c}{3} (\sqrt{2}\bar{\sigma}_x + \bar{\sigma}_y),$$

$$m_{s,88}^2 = m^2 + \frac{\lambda_1}{3} (5\bar{\sigma}_x^2 - 4\sqrt{2}\bar{\sigma}_x\bar{\sigma}_y + 7\bar{\sigma}_y^2) + \lambda_2 \left(\frac{\bar{\sigma}_x^2}{2} + 2\bar{\sigma}_y^2 \right) + \frac{\sqrt{2}c}{3} (\sqrt{2}\bar{\sigma}_x - \frac{\bar{\sigma}_y}{2}),$$

$$m_{s,08}^2 = \frac{2\lambda_1}{3} (\sqrt{2}\bar{\sigma}_x^2 - \bar{\sigma}_x\bar{\sigma}_y - \sqrt{2}\bar{\sigma}_y^2) + \sqrt{2}\lambda_2 \left(\frac{\bar{\sigma}_x^2}{2} - \bar{\sigma}_y^2 \right) + \frac{c}{3\sqrt{2}} (\bar{\sigma}_x - \sqrt{2}\bar{\sigma}_y).$$

- Pseudoscalars mesonic states

The squared masses for the pseudoscalar sector ($i = p$) read

$$m_{\pi}^2 = m^2 + \lambda_1 (\bar{\sigma}_x^2 + \bar{\sigma}_y^2) + \frac{\lambda_2}{2} \bar{\sigma}_x^2 - \frac{\sqrt{2}c}{2} \bar{\sigma}_y, \quad (39)$$

$$m_K^2 = m^2 + \lambda_1 (\bar{\sigma}_x^2 + \bar{\sigma}_y^2) + \frac{\lambda_2}{2} (\bar{\sigma}_x^2 - \sqrt{2}\bar{\sigma}_x\bar{\sigma}_y + 2\bar{\sigma}_y^2) - \frac{c}{2} \bar{\sigma}_x, \quad (40)$$

$$m_{\eta'}^2 = m_{p,00}^2 \cos^2 \theta_p + m_{p,88}^2 \sin^2 \theta_p + 2m_{p,08}^2 \sin \theta_p \cos \theta_p, \quad (41)$$

$$m_{\eta}^2 = m_{p,00}^2 \sin^2 \theta_p + m_{p,88}^2 \cos^2 \theta_p - 2m_{p,08}^2 \sin \theta_p \cos \theta_p, \quad (42)$$

with

$$m_{p,00}^2 = m^2 + \lambda_1 (\bar{\sigma}_x^2 + \bar{\sigma}_y^2) + \frac{\lambda_2}{3} (\bar{\sigma}_x^2 + \bar{\sigma}_y^2) + \frac{c}{3} (2\bar{\sigma}_x + \sqrt{2}\bar{\sigma}_y),$$

$$m_{p,88}^2 = m^2 + \lambda_1 (\bar{\sigma}_x^2 + \bar{\sigma}_y^2) + \frac{\lambda_2}{6} (\bar{\sigma}_x^2 + 4\bar{\sigma}_y^2) - \frac{c}{6} (4\bar{\sigma}_x - \sqrt{2}\bar{\sigma}_y),$$

$$m_{p,08}^2 = \frac{\sqrt{2}\lambda_2}{6} (\bar{\sigma}_x^2 - 2\bar{\sigma}_y^2) - \frac{c}{6} (\sqrt{2}\bar{\sigma}_x - 2\bar{\sigma}_y),$$

and the mixing angles are given by

$$\tan 2\theta_i = \frac{2m_{i,08}^2}{m_{i,00}^2 - m_{i,88}^2}, \quad i = s, p. \quad (43)$$

- The vectors mesonic states

Moreover, The squared masses for the vector sector ($i = V^\mu$) are given as

$$m_\rho^2 = m_1^2 + \frac{1}{2}(h_1 + h_2 + h_3)\bar{\sigma}_x^2 + \frac{h_1}{2}\bar{\sigma}_y^2 + 2\delta_x, \quad (44)$$

$$m_{K^*}^2 = m_1^2 + \frac{\bar{\sigma}_x^2}{4}(g_1^2 + 2h_1 + h_2) + \frac{\bar{\sigma}_x\bar{\sigma}_y}{\sqrt{2}}(h_3 - g_1^2) + \frac{\bar{\sigma}_y^2}{2}(g_1^2 + h_1 + h_2) + \delta_x + \delta_y, \quad (45)$$

$$m_{\omega_x}^2 = m_\rho^2, \quad (46)$$

$$m_{\omega_y}^2 = m_1^2 + \frac{h_1}{2}\bar{\sigma}_x^2 + \left(\frac{h_1}{2} + h_2 + h_3\right)\bar{\sigma}_y^2 + 2\delta_y, \quad (47)$$

- And finally the axial-vectors mesonic states

The squared masses for the axial-vector sector ($i = A^\mu$) are

$$m_{a_1}^2 = m_1^2 + \frac{1}{2}(2g_1^2 + h_1 + h_2 - h_3)\bar{\sigma}_x^2 + \frac{h_1}{2}\bar{\sigma}_y^2 + 2\delta_x, \quad (48)$$

$$m_{K_1}^2 = m_1^2 + \frac{1}{4}(g_1^2 + 2h_1 + h_2)\bar{\sigma}_x^2 - \frac{1}{\sqrt{2}}\bar{\sigma}_x\bar{\sigma}_y(h_3 - g_1^2) + \frac{1}{2}(g_1^2 + h_1 + h_2)\bar{\sigma}_y^2 + \delta_x + \delta_y, \quad (49)$$

$$m_{f_{1x}}^2 = m_{a_1}^2, \quad (50)$$

$$m_{f_{1y}}^2 = m_1^2 + \frac{\bar{\sigma}_x^2}{2}h_1 + \left(2g_1^2 + \frac{h_1}{2} + h_2 - h_3\right)\bar{\sigma}_y^2 + 2\delta_y. \quad (51)$$

The evolution of masses of (pseudo)-scalar states depends on the selected form of the anomaly term of $\mathcal{L}_{U(1)_A}$. This term causes anomaly in c -term. Choosing the anomaly term defines the description of the structure of the hadronic states [47]. The anomaly term, we worked with, agrees with the calculation of Refs. [21, 22, 60] but differs from Ref. [33]. Moreover, the estimated masses of (axial)-vector states are not affected by the anomaly term [33].

In evaluating the partition function, the quantum and thermal fluctuations of the mesonic fields are neglected. It is worthwhile to mention that the integration over the mesonic fields is renounced. Furthermore, the mesonic fields are replaced by their expectation values, σ_0 and σ_8 , resulting in the mesonic potential $U(\sigma_0, \sigma_8)$. The quarks are treated as quantum fields. The integration over the quark fields yields a determinant, which can be rewritten as a trace over a logarithm defined by Eq. (25) for LSM and Eq. (30) for PLSM. The Matsubara formalism [66] gives an estimation for the quark contribution to the meson masses, section V.

In order to include the quark contribution in the grand potential, the mesonic masses should be modified due to the in-medium effects of finite temperature. In order to calculate the second derivative, Eq. (34), corresponding to LSM where we take into account Eq.

(25) and diagonalize the resulting quark mass matrix, we can derive an expression for the modification in the mesonic masses [21].

$$m_{i,ab}^2 = \left. \frac{\partial^2 \Omega(T, \mu_f)}{\partial \zeta_{i,a} \partial \zeta_{i,b}} \right|_{\min} = \nu_c \sum_{f=l,s} \int \frac{d^3 p}{(2\pi)^3} \frac{1}{2E_{q,f}} \left[(n_{q,f} + n_{\bar{q},f}) \left(m_{f,ab}^2 - \frac{m_{f,a}^2 m_{f,b}^2}{2E_{q,f}^2} \right) - (b_{q,f} + b_{\bar{q},f}) \left(\frac{m_{f,a}^2 m_{f,b}^2}{2E_{q,f} T} \right) \right]. \quad (52)$$

The quark mass derivative with respect to the meson fields $\zeta_{i,a}$, $m_{f,a}^2 \equiv \partial m_f^2 / \partial \zeta_{i,a}$ and that with respect to the meson fields $\zeta_{i,a} \partial \zeta_{i,b}$, $m_{f,ab}^2 \equiv \partial m_f^2 / \partial \zeta_{i,a} \partial \zeta_{i,b}$ are listed in Tab. II. Correspondingly, the antiquark function $b_{\bar{q},f}(T, \mu_f) = b_{q,f}(T, -\mu_f)$, where

$$b_{q,f}(T, \mu_f) = n_{q,f}(T, \mu_f)(1 - n_{q,f}(T, \mu_f)). \quad (53)$$

A expression for the meson mass modification can be estimated from PLSM, Eq. (30), and the diagonalization of the resulting quark mass matrix [22],

$$m_{i,ab}^2 = \left. \frac{\partial^2 \Omega(T, \mu_f)}{\partial \zeta_{i,a} \partial \zeta_{i,b}} \right|_{\min} = \nu_c \sum_{f=l,s} \int \frac{d^3 p}{(2\pi)^3} \frac{1}{2E_{q,f}} \left[(N_{q,f} + N_{\bar{q},f}) \left(m_{f,ab}^2 - \frac{m_{f,a}^2 m_{f,b}^2}{2E_{q,f}^2} \right) + (B_{q,f} + B_{\bar{q},f}) \left(\frac{m_{f,a}^2 m_{f,b}^2}{2E_{q,f} T} \right) \right]. \quad (54)$$

The definitions, $E_{q,f}(T, \mu) = E_{q,f}(T, -\mu)$ and

$$N_{q,f} = \frac{\Phi e^{-E_{q,f}/T} + 2\Phi^* e^{-2E_{q,f}/T} + e^{-3E_{q,f}/T}}{1 + 3(\phi + \phi^* e^{-E_{q,f}/T}) e^{-E_{q,f}/T} + e^{-3E_{\bar{q},f}/T}}, \quad (55)$$

$$N_{\bar{q},f} = \frac{\Phi^* e^{-E_{\bar{q},f}/T} + 2\Phi e^{-2E_{\bar{q},f}/T} + e^{-3E_{\bar{q},f}/T}}{1 + 3(\phi^* + \phi e^{-E_{\bar{q},f}/T}) e^{-E_{\bar{q},f}/T} + e^{-3E_{q,f}/T}}, \quad (56)$$

are implemented [22].

For quark, $B_{q,f} = 3(N_{q,f})^2 - C_{q,f}$ and for antiquark, $B_{\bar{q},f} = 3(N_{\bar{q},f})^2 - C_{\bar{q},f}$,

$$C_{q,f} = \frac{\Phi e^{-E_{q,f}/T} + 4\Phi^* e^{-2E_{q,f}/T} + 3e^{-3E_{q,f}/T}}{1 + 3(\phi + \phi^* e^{-E_{q,f}/T}) e^{-E_{q,f}/T} + e^{-3E_{\bar{q},f}/T}}, \quad (57)$$

$$C_{\bar{q},f} = \frac{\Phi^* e^{-E_{\bar{q},f}/T} + 4\Phi e^{-2E_{\bar{q},f}/T} + 3e^{-3E_{\bar{q},f}/T}}{1 + 3(\phi^* + \phi e^{-E_{\bar{q},f}/T}) e^{-E_{\bar{q},f}/T} + e^{-3E_{q,f}/T}}, \quad (58)$$

are defined [22].

The quark masses has to be taken into account and accordingly same isospin of light quarks $m_u = m_d$. but different for m_s . The first and second derivatives of squared quark mass in non-strange and strange basis with respect to meson fields are evaluated at minimum [21]. In Tab. II, the summation over the two light flavors, denoted by symbol l , are in given in

the first two columns present the first and second derivatives of squared light quark masses, respectively. The last two columns are devoted to the strange quark mass. In spite of the consideration of $SU(2)$ isospin symmetry, the derivatives the first and second derivatives of squared light quark masses are different for the u - and d -quark, where their summation is cancelled out [21].

	$m_{l,a}^2 m_{q,b}^2 / g^4$	$m_{l,ab}^2 / g^2$	$m_{s,a}^2 m_{s,b}^2 / g^4$	$m_{s,ab}^2 / g^2$
$\sigma_0 \sigma_0$	$\frac{1}{3} \sigma_x^2$	$\frac{2}{3}$	$\frac{1}{3} \sigma_y^2$	$\frac{1}{3}$
$\sigma_1 \sigma_1$	$\frac{1}{2} \sigma_x^2$	1	0	0
$\sigma_4 \sigma_4$	0	$\sigma_x \frac{\sigma_x + \sqrt{2} \sigma_y}{\sigma_x^2 - 2\sigma_y^2}$	0	$\sigma_y \frac{\sqrt{2} \sigma_x + 2\sigma_y}{2\sigma_y^2 - \sigma_x^2}$
$\sigma_8 \sigma_8$	$\frac{1}{6} \sigma_x^2$	$\frac{1}{3}$	$\frac{2}{3} \sigma_y^2$	$\frac{2}{3}$
$\sigma_0 \sigma_8$	$\frac{\sqrt{2}}{6} \sigma_x^2$	$\frac{\sqrt{2}}{3}$	$-\frac{\sqrt{2}}{3} \sigma_y^2$	$-\frac{\sqrt{2}}{3}$
$\pi_0 \pi_0$	0	$\frac{2}{3}$	0	$\frac{1}{3}$
$\pi_1 \pi_1$	0	1	0	0
$\pi_4 \pi_4$	0	$\sigma_x \frac{\sigma_x - \sqrt{2} \sigma_y}{\sigma_x^2 - 2\sigma_y^2}$	0	$\sigma_y \frac{\sqrt{2} \sigma_x - 2\sigma_y}{\sigma_x^2 - 2\sigma_y^2}$
$\pi_8 \pi_8$	0	$\frac{1}{3}$	0	$\frac{2}{3}$
$\pi_0 \pi_8$	0	$\frac{\sqrt{2}}{3}$	0	$-\frac{\sqrt{2}}{3}$

Tab. II: The first and second derivatives of the squared quark mass in non-strange (first two columns) and strange (last two columns) basis with respect to the meson fields are evaluated at minimum [21].

Tab. III presents a comparison between the different scalar and vector meson nonets in various effective thermal models, like PLSM (present work) and PNJL [25] confronted to the particle data group [28] and lattice QCD calculations [26, 27]. Some remarks are now in order. The errors are deduced from the fitting for the parameters used in calculating the equation of states and other thermodynamics quantities. The fitting requires information from the experimental data regarding both (axial)-vector and (pseudo)-scalar states. The output results are very precise for some of the lightest hadron resonances described by the present model, PLSM. We aim to describe hadron vacuum phenomenology with such an extreme precision and not only to describe the hadron spectrum in both thermal- and hadronic dense-medium. We show the effects of the chiral condensate and deconfinement phase-transition in order to characterize the chiral phase-structure of many hadrons. The PNJL model is limited to study (pseudo)-scalar meson states. Only pseudoscalar and vector

Sector	Symbol	PDG [28]	PLSM	PNJL [24, 25]	Lattice QCD	
					Hot QCD[26]	PACS-CS [27]
Scalar $J^{PC} = 0^{++}$	a_0	$a_0(980^{\pm 20})$	1026	837		
	κ	$K_0^*(1425^{\pm 50})$	1115	1013		
	σ	$\sigma(400 - 1200)$	800	700		
	f_0	$f_0(1200 - 1500)$	1284	1169		
Pseudoscalar $J^{PC} = 0^{-+}$	π	$\pi^0(134.97^{\pm 6.9})$	120	126	$134^{\pm 6}$	$135.4^{\pm 6.2}$
	K	$K^0(497.614^{\pm 24.8})$	509	490	$422.6^{\pm 11.3}$	$498^{\pm 22}$
	η	$\eta(547.853^{\pm 27.4})$	553	505	$579^{\pm 7.3}$	$688^{\pm 32}$
	η'	$\eta'(957.78^{\pm 60})$	965	949	—	—
Vector $J^{PC} = 1^-$	ρ	$\rho(775.49^{\pm 38.8})$	745	—	$756.2^{\pm 36}$	$597^{\pm 86}$
	ω_X	$\omega(782.65^{\pm 44.7})$	745	—	$884^{\pm 18}$	$861^{\pm 23}$
	K^*	$K^*(891.66^{\pm 26})$	894	—	$1005^{\pm 93}$	$1010.2^{\pm 77}$
	ω_y	$\phi(1019.455^{\pm 51})$	1005	—	—	—
Axial-Vector $J^{PC} = 1^{++}$	a_1	$a_1(1030 - 1260)$	980	—		
	f_{1x}	$f_1(1281^{\pm 60})$	980	—		
	K_1^*	$K_1^*(1270^{\pm 7})$	1135	—		
	f_{1y}	$f_1(1420^{\pm 71.3})$	1315	—		

Tab. III: A comparison between (pseudo)-scalar and (axial)-vector meson sectors in PLSM (present work) and the corresponding results from PNJL [25]. Both are compared with the experimental measurements, the Particle Data Group (PDG) [28] and the lattice QCD simulations [26, 27].

meson masses are available in the lattice QCD calculations (HotQCD Collaboration) [26] and (PACS-CS Collaboration) [27].

The estimation of masses seems to agree well with Refs. [21, 22, 33, 60]. But for mixing strange with nonstrange scalar states, one state < 1 GeV and another one > 1 GeV were obtained in Ref. [33]. The authors should implement Gyuri fit to correct this [51].

1. Temperature Dependence

In the presence of chiral symmetry breaking and the correction of Polyakov loop potential, we present different scalar and vector meson nonets in thermal- and hadronic dense-medium

and estimate the corresponding meson spectrum. We start with the mesonic masses at finite temperature and varying baryon chemical potential in both LSM and PLSM. The thermal evolution for scalar and pseudoscalar are shown in figs. 5 and 6, respectively. The vector and axial-vector are presented in Fig. 7. In the same way, the mass spectrum at nonzero chemical potential in both LSM and PLSM in dense-medium are shown in Figs. 8 and 9 for scalar, pseudoscalar mesons and in Fig. 10 for vector and axial-vector mesons.

The temperature variations of mesonic masses can be understood as the in-medium thermal effects on the mesonic states. As shown in Figs. 5 and 6, respectively, the bosonic thermal contributions to the mesonic masses decrease with increasing the temperature, while the fermionic contributions increase at high temperatures. The fermionic (quark) contributions are negligible at small temperatures. At high temperatures, the bosonic thermal contributions dominates. This leads to degeneration in the mesonic masses, which in turn leads to a nature change in chiral and deconfinement phase-transition with increasing temperature.

In Fig. 5, the left-hand panel shows the two scalar meson sectors, a_0 , σ and the two pseudoscalar meson sectors, η' and π , in thermal hadronic medium at vanishing baryon chemical potentials μ in the presence of $U(1)_A$ symmetry breaking. The $U(1)_A$ symmetry breaking gets effectively restored and repeals the mass gap between the chiral partners [21], where at very large temperatures comparable to the strange quark mass, the difference between the strange and non-strange mesons becomes negligible, Fig. 2. Accordingly, all mesonic masses will degenerate. Since at very high temperature, the major effect takes place in the strange mass, such as a_0 and η' the masses of σ and π degenerate in close vicinity of reduced temperature. This result is compatible with the result reported in Ref. [21]. The masses of a_0 and $\eta' \sim 250$ MeV and masses of σ and $\pi \sim 181$ MeV. The term with $U(1)_A$ symmetry breaking appears in the meson masses through the c anomaly breaking term. It is strongly related to the strange condensate σ_y . In right-hand panel, the Poyakov-loop correction is introduced. This correction seems to enhance the quark dynamics and raise the mass degeneration in a sharp and fast way.

In Fig. 5, the different panels present an systematic study of the effects of the chemical potentials on the sixteen mesonic states. We find that increasing the chemical potential (from top to bottom panels) enhances the degeneration of the mesonic masses. For example, at $\mu = 100$ MeV, four meson states a_0 , η' become degenerate at ~ 240 MeV, σ and π at ~ 180 , while at $\mu = 220$ the four states a_0 , η' degenerate at ~ 170 MeV, σ and π at ~ 125 MeV. This has a strong relationship with the chiral condensate and the deconfinement phase-transition.

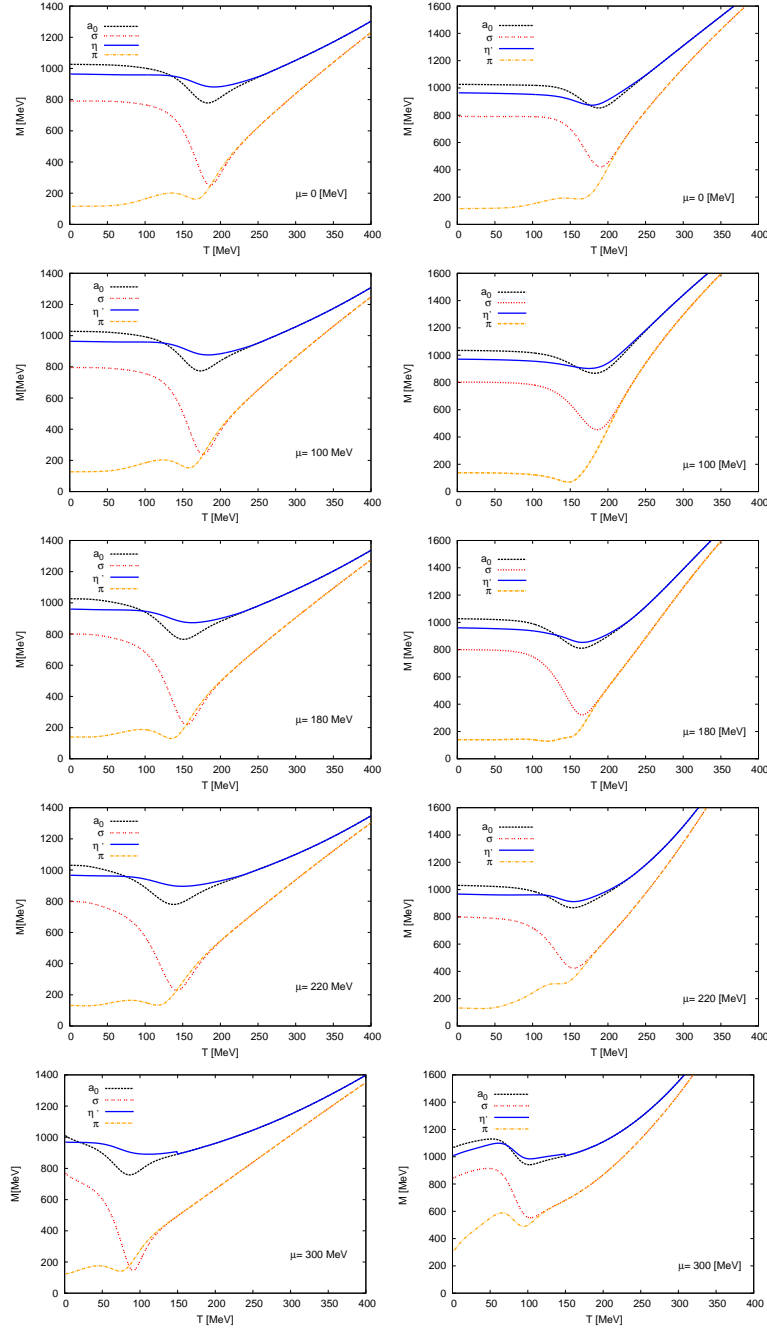


Fig. 5: (Color online) Scalar a_0 (dashed curve) and σ (dotted curve) and pseudoscalars states η (solid curve) and π (dashed-dotted curve) are given as functions of temperature at different chemical potentials $\mu = 0, 100, 180, 220$ and 300 MeV. Left-hand panel shows LSM results. The PLSM are presented in the right-hand panel.

In Fig. 3, the chiral condensates $\bar{\sigma}_x$ and $\bar{\sigma}_y$ and deconfinement phase-transition ϕ and ϕ^* vary with T and μ . The contributions from the non-strange quarks to the rapid crossover in the non-strange sector are different and affect the contributions of the mesonic masses,

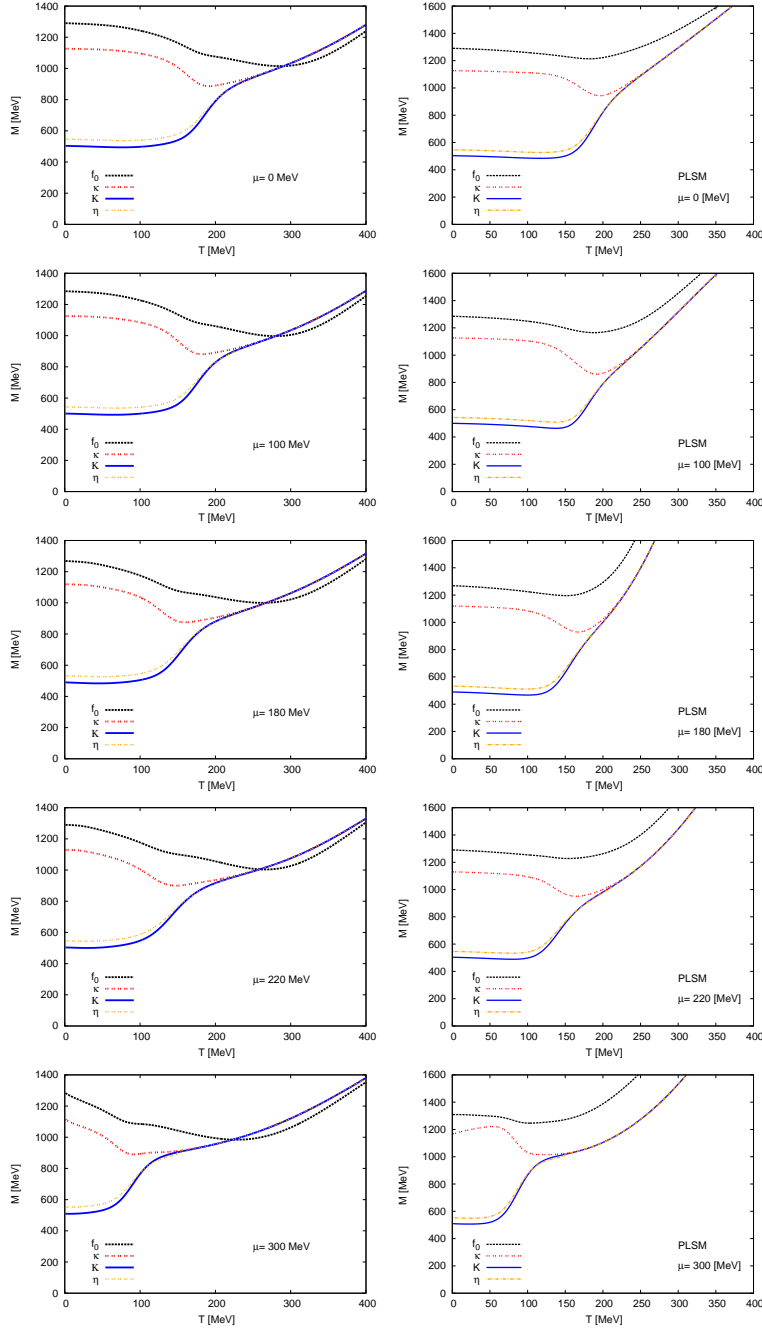


Fig. 6: (Color online) Left-hand panel (LSM) and right-hand panel (PLSM): scalars f_0 (horizontal dashed curve) and κ (vertical dashed curve) and pseudoscalars η (dotted curve) and K (solid curve) are given in dependence on the temperature at different chemical potentials $\mu = 0, 100, 180, 220$ and 300 MeV.

very strongly [21].

Fig. 6 presents the thermal evolution of scalars f_0 (horizontal dashed curve) and κ (vertical dashed curve) and pseudoscalars η (dotted curve) and K (solid curve) at different chemical potentials $\mu = 0, 100, 180, 220$ and 300 MeV. We find that the masses of these

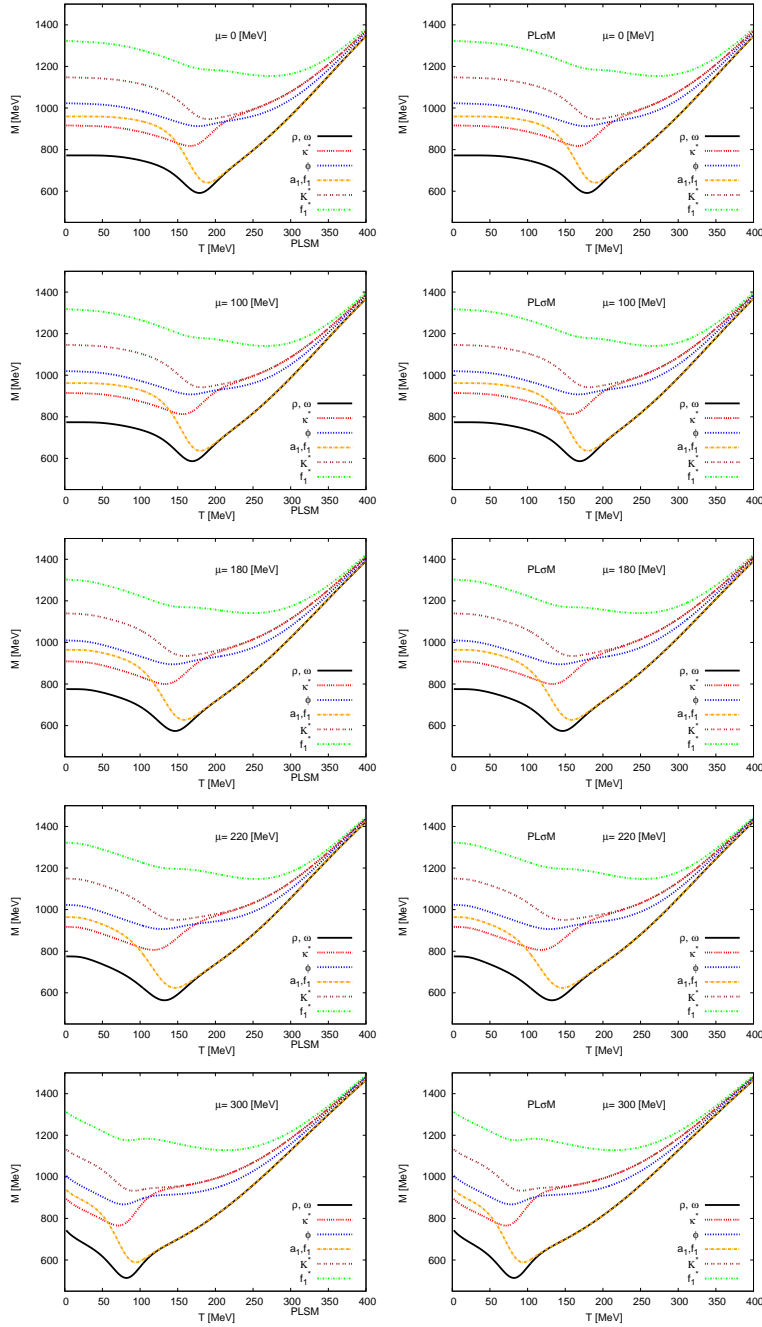


Fig. 7: (Color online) Left-hand panel (LSM) and right-hand panel (PLSM): vector mesons ρ and ω (solid curve), κ^* (log dotted curve) and ϕ (dotted curve) and axial-vector mesons $a_1 = f_1$ (dashed-dotted curve), K^* (dotted curve) and f_1^* (short dashed-dotted curve) are given in T -dependence at different chemical potentials $\mu = 0, 100, 180, 220$ and 300 MeV.

states degenerate at $T \sim 240$ MeV, especially in LSM. In the same way as shown in Fig. 5 for example, at $\mu = 100$ MeV, the temperatures at which the three mesonic states κ, K and η , become degenerate $T \sim 240$. Strength of the stability state at low temperatures delays

as the density increases.

The left-hand panel of Fig. 7 gives the thermal evolution of ρ , ω , a_1 , f_1 , κ^* , K^* and ϕ calculated in the LSM. We find that the masses of these states degenerate at $T \sim 200$ MeV, while κ^* , K^* and ϕ at $T \sim 240$ MeV. At high temperatures, it is obvious that the effects of the non-strange mass vanish. This makes the differences between the various masses disappear. Increasing the chemical potential reduces the temperatures, at which the masses degenerate. This can be understood on the basis of the thermal evolution of the chiral condensates and the deconfinement phase-transition, shown in Fig. 3. At $\mu = 300$ MeV, ρ , ω , a_1 and f_1 degenerate at $T \sim 110$ MeV, while κ^* , K^* and ϕ degenerate at $T \sim 140$ MeV. The right-hand panel presents the same results but calculated in PLSM. The Poyakov loop-correction causes sharp and fast mass degeneration.

The mass degeneration can be interpreted as the effect of the fermionic vacuum fluctuations on the chiral symmetry restoration [21], especially on the condensate σ_y . The effect melts the strange condensate faster than the non-strange one σ_x , Fig. (1). At very high temperature, the mass gap between mesons seems to disappear and decrease with the melting strange condensate σ_y . This mass gap appears at low temperatures, where the non-strange condensate remains finite. At temperatures higher than the critical value only strange condensate remains finite. This thermal effects is strongly related to the degeneration of the meson masses.

2. Density Dependence

The meson masses are shown for the case with $U(1)_A$ anomaly as a function of chemical potential at different temperatures in LSM (left-hand panel) and PLSM (right-hand panel), where the scalar and pseudoscalar are shown in Figs. 8 and 9 while the vector and axial-vector mesons are depicted in Fig. 10.

In left-hand panel of Fig. 8, we notice that all masses keep their vacuum values almost unchanged until the chemical potential reaches the Fermi surface for the light quarks [67] at $\mu \sim 350$ MeV. The mass of σ meson drops below the mass of π meson at the value where the first-order transition should be located [67]. This means that the masses of pseudoscalar mesons stay nearly constant until the phase transition, Fig. 8, while the scalar mesons show a stronger melting behavior above the Fermi surface for the light quarks [67]. The right-hand panel presents the effects of the Poyakov loop-correction introduced to the quark

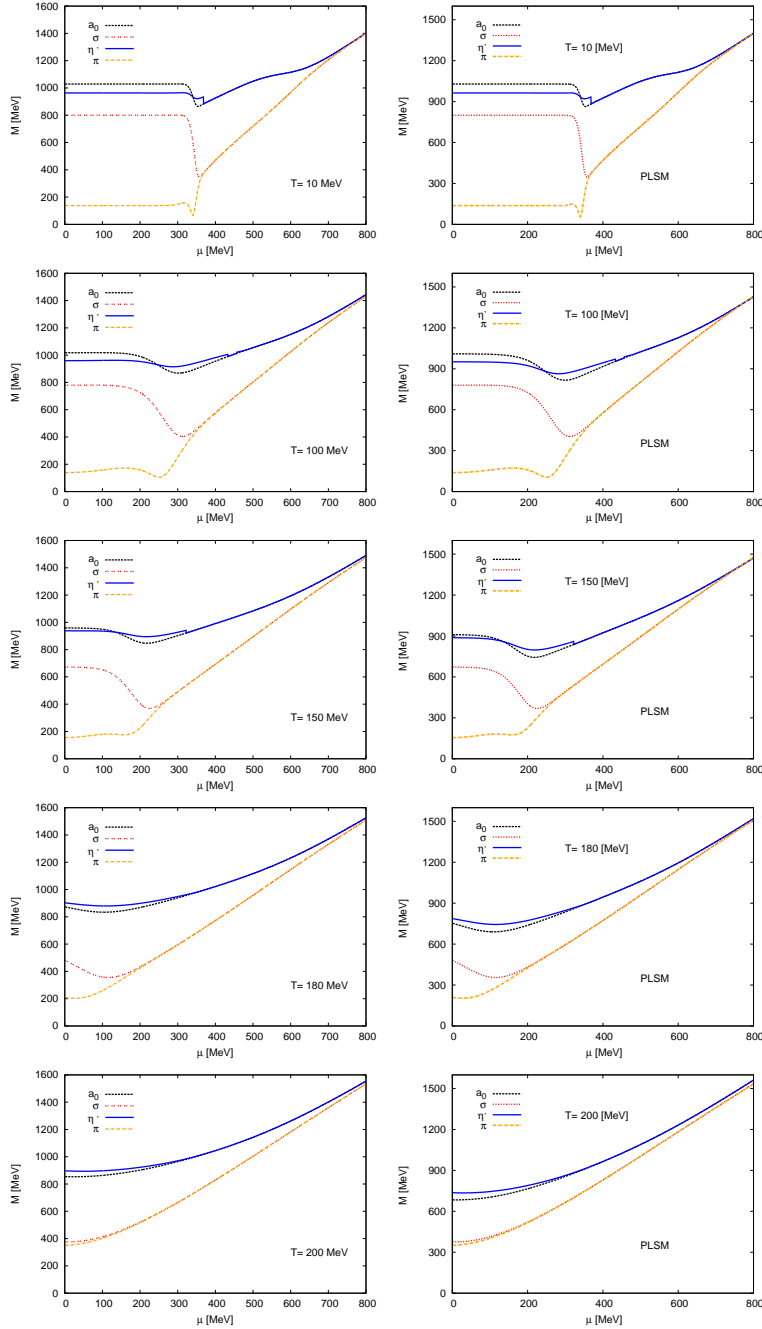


Fig. 8: (Color online) Left-hand panel (LSM) and right-hand panel (PLSM) presents scalars a_0 (dashed curve) and σ (dotted curve) and pseudoscalars η' (solid curve) and π (dashed-dotted curve) in hadronic dense medium at fixed temperatures $T = 10, 100, 150, 180$ and 200 MeV.

dynamics. This causes a sharp transition in the mass degeneration. The increase of the melting behavior above T_c derives the masses to be compacted with each other.

In left-hand panel of Fig. 9, we find that all masses stay at their vacuum values until the chemical potential reaches the Fermi surface for the light quarks at $\mu \sim 350$ MeV. The meson masses drops at the first-order transition and κ meson drops below to the masses of

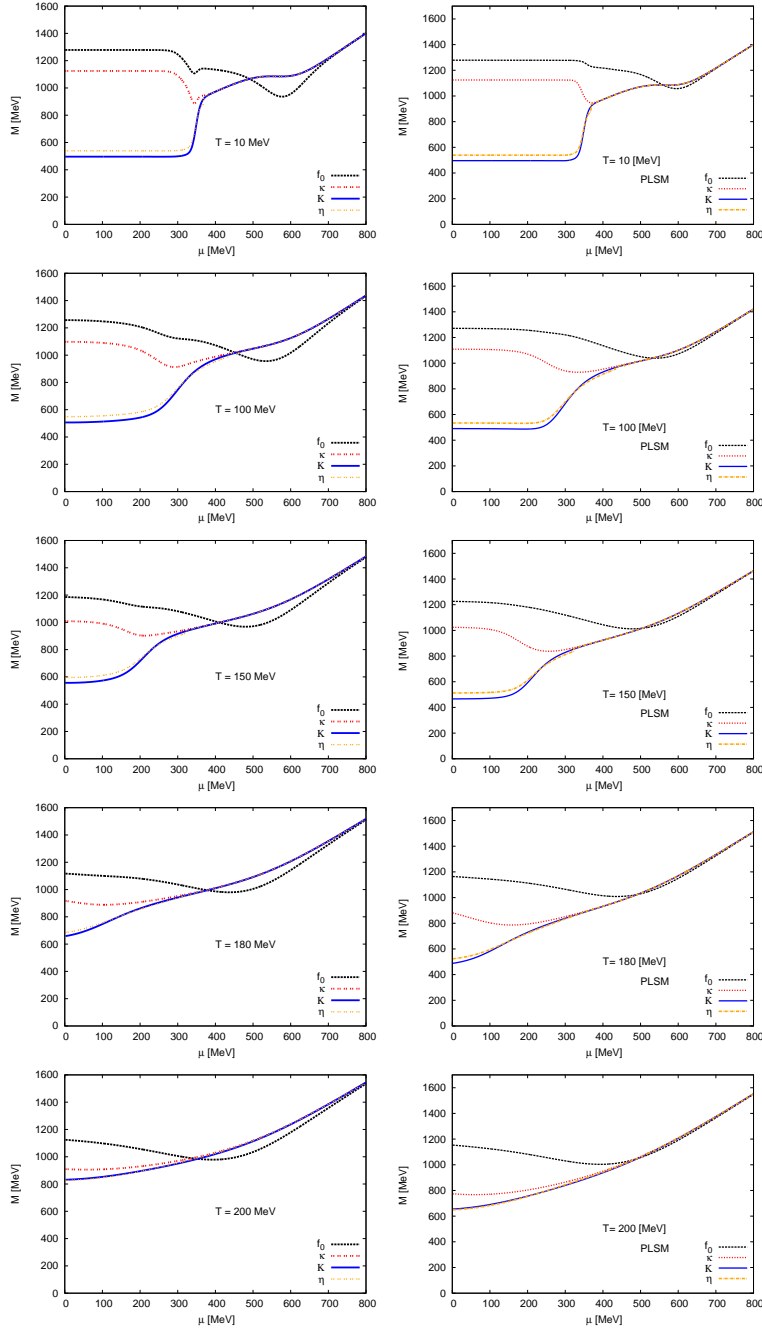


Fig. 9: (Color online) Left-hand panel (LSM) and right-hand panel (PLSM) show scalars f_0 (horizontal dashed curve) and κ (vertical dashed curve) and pseudoscalars η (dotted curve) and K (solid curve) in hadronic dense medium at fixed temperatures $T = 10, 100, 150, 180$ and 200 MeV.

K and η mesons. Only in the curve for f_0 meson, the Fermi surface for the strange quarks is clearly visible. The mass of f_0 decreases below κ . Masses of K and η decreases only after the light quark phase transition (this the second phase transition) and degenerates with other meson masses at very high chemical potential $\mu = 700$ MeV. These value decrease as the

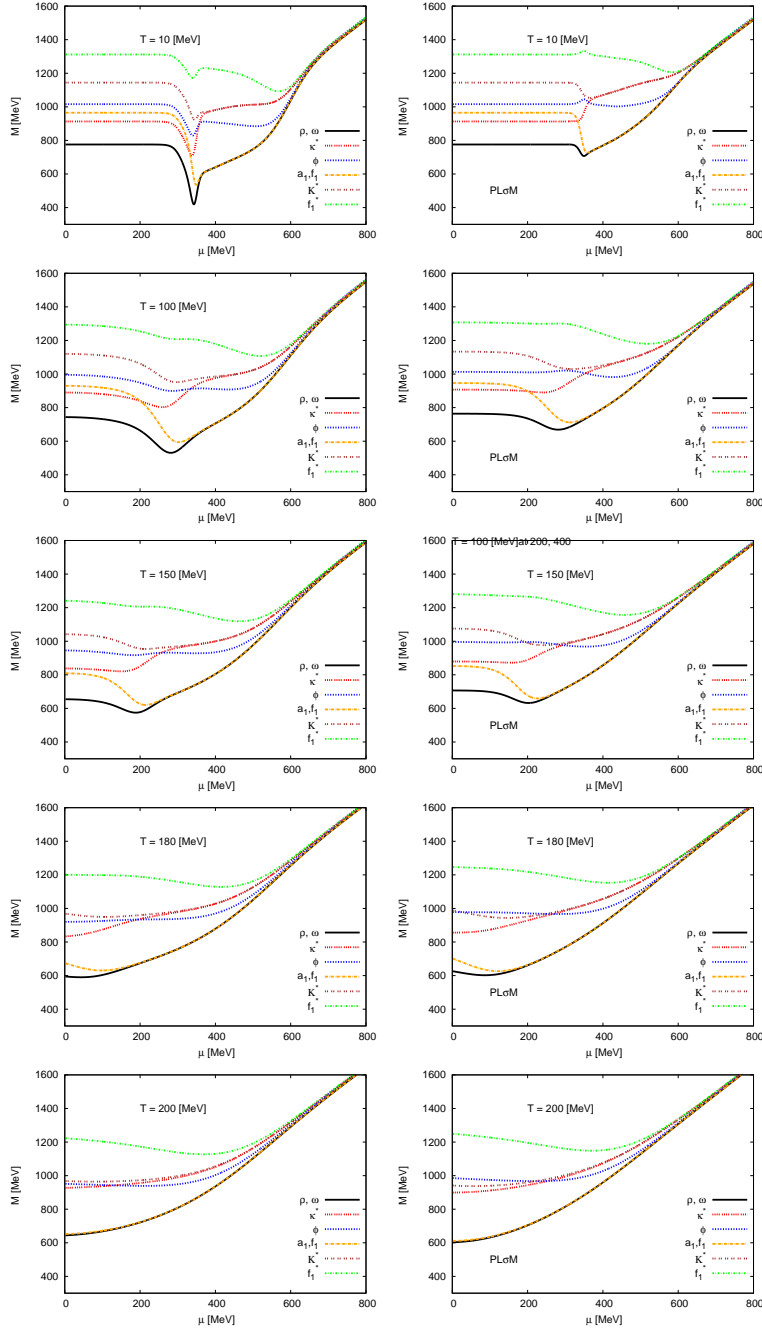


Fig. 10: (Color online) Left-hand panel (LSM) and right-hand panel (PLSM) shows vector mesons ρ , ω (solid curve), κ^* (log dotted curve) and ϕ (dotted curve) and axial-vector mesons $a_1 = f_1$ (dashed-dotted curve), K^* (dotted curve) and f_1^* (short dashed-dotted) in hadronic dense medium at different temperatures $T = 10, 100, 150, 180$ and 200 MeV.

melting point of the system increases. The first slight drop of f_0 meson takes place at $\mu \sim 350$ MeV, due to the induced drop in the strange condensate. The right-hand panel shows the Ployakov loop-correction introduced the quark dynamics. Apparently, this enhances the

mass degeneration through the deconfinement phase-transition to appear sharper and faster than LSM.

Fig. 10 shows the LSM (right-hand panel) and PLSM (right-hand panel) results of vector and axial-vector mesons as functions of the chemical potentials at different fixed temperatures. This gives a systematic study for the variation of heating effect on the hadronic dense medium. In the left-hand panel we find that the axial-vector, a_1 and f_1 keeps their vacuum values till $\mu = 350$ MeV. Then, they drop below to the vector mesons ρ and ω . This is accompanied by strong phase-transition (first-order) and degeneration of their masses. The axial-vector meson K^* keeps its vacuum value till the same value of chemical potential. Then it drops below to vector meson ρ and ω . In this case, this is accompanied by a phase transition (first order). The strange meson states f_1^* and ϕ degenerate only at very high chemical potential, $\mu \sim 700$ MeV. These μ -values decrease with increase T . Increase T reduces chemical potentials at which the degeneration gets compatible with the previous cases and easily gaps the Fermi surface for the light quarks. These would mean that the masses of vector mesons stay nearly constant until the phase transition, while the masses of the axial-vector mesons show a stronger melting above the Fermi surface for the light quarks.

The right-hand panel Fig. 10 shows the in-medium effect of chemical potential (density) on the vector and axial-vector mesons in the presence of Ployakov loop-correction and symmetry breaking. We find that the deconfinement phase-transition has considerable effects on the chiral phase-transition in meson masses, where the restoration of the chiral symmetry becomes sharper and faster than the LSM. For example, very close to the critical temperature, $T = 180$ MeV, the axial-vector mesons a_1 and f_1 keep their vacuum values till $\mu \sim 180$ MeV. Then, the two masses become smaller than that of the vector mesons ρ and ω . The axial-vector meson, K^* , keeps its vacuum value till $\mu \sim 300$ MeV. Then, its mass drops below the ones of the vector mesons ρ and ω . At a characteristic value of the chemical potential, the masses of all meson groups degenerate with each other.

Comparison	Scalar mesons	Pseudoscalar mesons	Vector mesons	Axial-vector mesons
meson	$a_0 \ \kappa \ \sigma \ f_0$	$\pi \ K \ \eta \ \eta'$	$\rho \ K_0^* \ \omega \ \phi$	$a_1 \ K_1 \ f_1 \ f_1^*$
$T_{Dissolving}^{Meson}$ [MeV]	200 250 320 320	320 230 235 300	195 300 195 300	205 250 205 350

Tab. IV: The approximate dissolving temperature corresponding to meson sectors.

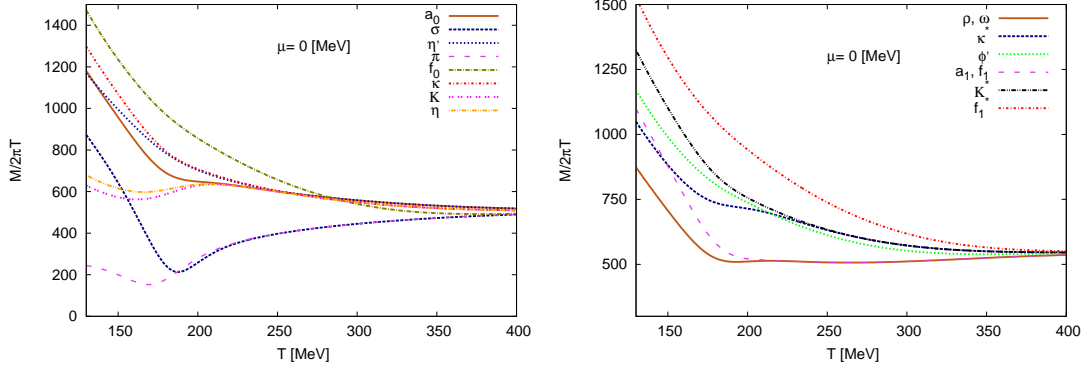


Fig. 11: (Color online) The left-hand panel shows scalar/pseudoscalar meson sectors in hadronic thermal medium at vanishing chemical potential, while the right-hand panel refers to the vector/axial-vector meson sectors.

B. Exclusion of Anomalous Terms

The axial anomalous term $U(1)_A$ is considered by an effective t'Hooft determinant in the Lagrangian, which breaks $U(1)_A$ symmetry [2, 68]. This term appears in the anomaly Lagrangian Eq. (5), and in the pure mesonic potential, Eq. (31), through the parameter c . Eliminating this term likely affects the chiral phase-transition and plays an essential role on phenomenology of scalar and pseudoscalar masses at finite temperature and density. The vector and axialvector masses are not affected by the anomalous term, Eqs. (44)-(51). It is conjectured that the axial anomaly-breaking term is constant (not depending on temperature and chemical potential) [21]. In this section, we introduce the influence of the axial anomaly on the meson masses.

In case that the anomalous terms depend on the temperature, this leads to fast effective-restoration of the axial symmetry [21]. It was found that the anomalous term decreases with increasing temperature [21]. At very high temperatures, both condensates σ_x and σ_y likely degenerate [21].

In case that the condensates depend on the chemical potential, we find that the upper Fermi surface of the light quarks coincides with the light quark mass, $\mu \approx m_l = 300$ MeV, where the chiral condensates are in the broken phase (below the phase transition) and the strange condensate has no influence on the axial anomaly [21]. The phase transition is mainly estimated by the nonstrange condensate σ_x , while the leap in the strange condensate σ_x can be neglected. Below Fermi surface (above the phase transition), the strange condensate should be taken into account $\mu \approx m_g = 433$ MeV.

1. Temperature Dependence

The thermal evolution of the meson states in the case of negligible influence of the axial anomaly term $U(1)_A$ at vanishing chemical potential $\mu = 0.0$ MeV, LSM (left-hand panel) and PLSM (right-hand panel), in Fig. 12, show that the critical temperature T_c remains unchanged, the mass gap between the chiral partners vanishes in the restored phase and all meson states begin to be degenerate at the light chiral restoration T_c^q temperature. This value of T_c does not change by introducing the anomaly term. The introduction of the color and gluon dynamics in form of Polyakov loop accelerates of the a_0 and σ states to η' and π .

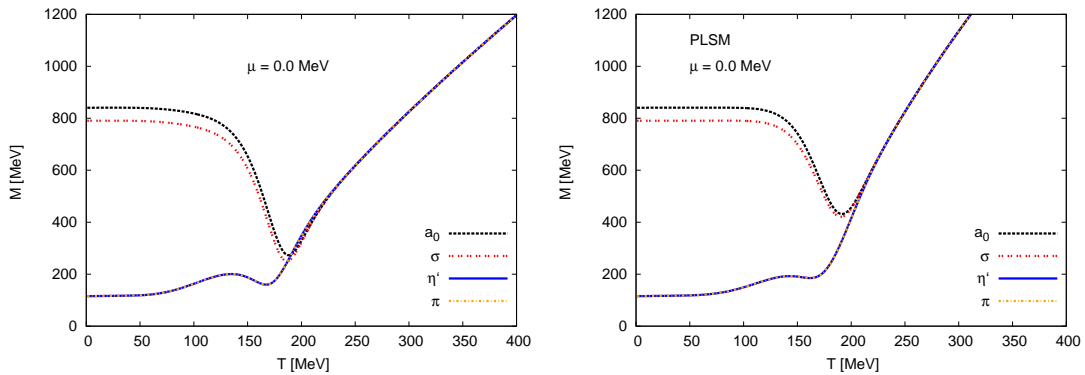


Fig. 12: (Color online) Left- (LSM) and right-hand panel (PLSM) show scalar a_0 (dashed curve) and σ (dotted curve) and pseudoscalar states η' (solid curve) and π (dashed-dotted curve) as functions of temperature at vanishing chemical potentials $\mu = 0.0$ MeV.

Figure 13 shows that the chiral restoration remains not complete till certain temperature value exceed the critical temperature of the light chiral restoration. It is obvious that the four meson states degenerate at same approximate temperature in presence of the axial anomaly term. The chiral restoration is not fully because η degenerates with κ and K at a value which is larger than that of the light chiral restoration, T_c^q . These values are not changed in both cases, i.e. with/without anomaly and the introduction of the color and gluon interaction increase the value.

2. Density Dependence

The density evolution of mesonic states in case of negligible influence of the axial anomaly term $U(1)_A$ at finite temperate is evaluated at $T = 10.0$ MeV in LSM (left-hand panel) and

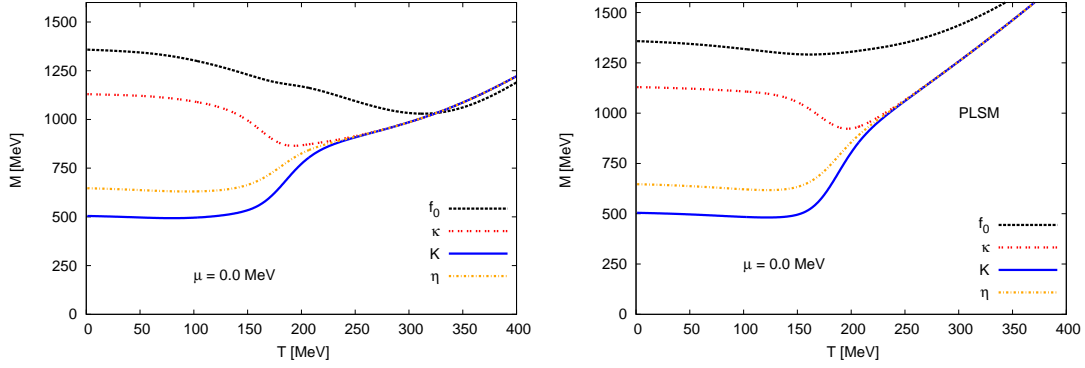


Fig. 13: (Color online) Left- (LSM) and right-hand panel (PLSM) show scalars f_0 (horizontal dashed curve) and κ (vertical dashed curve) and pseudoscalars η (dotted curve) and K (solid curve) as functions of temperature at vanishing chemical potentials $\mu = 0.0$ MeV.

PLSM (right-hand panel) in Fig. 14. The critical temperature does not change from the case, where the axial anomaly term is included. But the introduction of the color dynamics in absence of axial anomaly term appears well in left-hand panel of Fig. 14. The limit of the Fermi surface is unchanged in both cases with and without anomaly. In Fig. 14, the drops of a_0 and σ states to η' and π states are slowly. This is sharp and localized in a small region around the critical μ_c . The phase transition is first order. This means that the scalar mesons show a stronger melting behavior, while the introduction of the color dynamics of quarks bears out the pseudoscalar states to be have large melting point as shown in left-hand panel of Fig. 14. The degenerate state between all four meson masses is assumed to take place at the second order phase-transition.

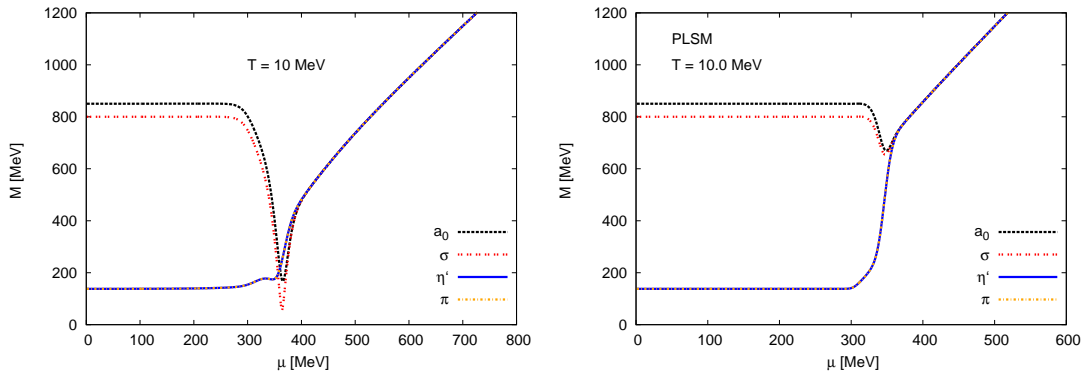


Fig. 14: (Color online) Left- (LSM) and right-hand panel (PLSM) present scalars a_0 (dashed curve) and σ (dotted curve) and pseudoscalars η' (solid curve) and π (dashed-dotted curve) in dense medium at fixed temperature $T = 10$ MeV.

In Fig. 15, κ state drops to K and η states in a first order phase-transition, but the chiral

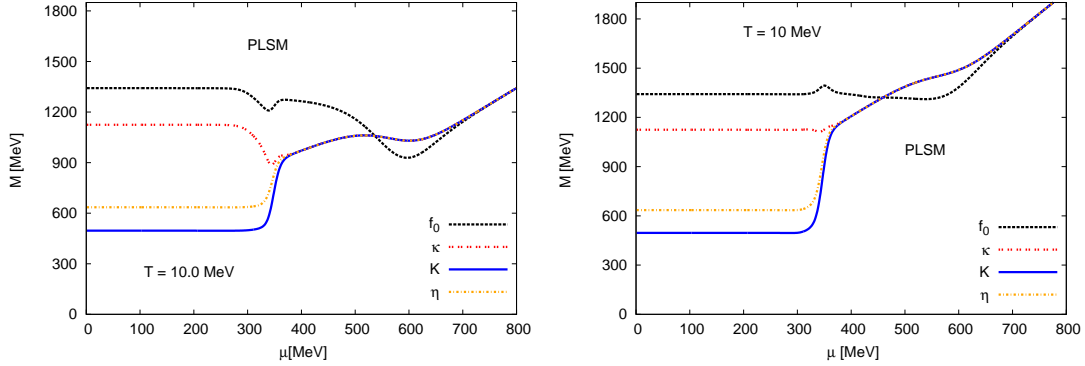


Fig. 15: (Color online) Left- (LSM) and right-hand panel (PLSM) show scalars f_0 (horizontal dashed curve) and κ (vertical dashed curve) and pseudoscalars η (dotted curve) and K (solid curve) in dense medium at fixed temperature $T = 10$ MeV.

phase-restoration will not complete till the f_0 degenerates at higher order phase-transition. All properties obtained in anomaly case were appeared in this case where anomalous terms are excluded.

C. Numerical Parameters of the Model

Table V summarizes the numerical values of the various parameters of the model used in this work in order to deduce thermal and density evolution of the scalar and pseudoscalar meson masses [21]. Here, it is distinguished between the case where the anomalous terms, c , are finite and vanishing.

Table VI summarizes the numerical values of the various parameters of the model used in this work in order to deduce thermal and density evolution of the vector and axial-vector meson masses [21].

	c [MeV]	h_x [MeV ³]	h_y [MeV ³]	m^2 [MeV ²]	λ_1	λ_2	g
With anomaly	4807.84	$(120.73)^3$	$(336.41)^3$	$-(306.26)^2$	13.49	46.48	6.5
Without anomaly	0	$(120.73)^3$	$(336.41)^3$	$-(503.55)^2$	-4.55	82.47	6.5

Tab. V: Scalar/pseudoscalar: the numerical values of the parameters used in the calculations [21].

	h_1	h_2	h_3	$m_1^2[MeV^2]$	$\delta_x[MeV^2]$	$\delta_y[MeV^2]$	g_1
Vector/axial-vector	0	9.87	4.8667	$(0.4135)^2$	0	$(0.1511)^2$	6.5

Tab. VI: Vector/axial-vector: the numerical values of the parameters used in the calculations [33].

V. NORMALIZATION TO THE LOWEST MATSUBARA FREQUENCY

In finite temperature field theory, the Matsubara frequencies are a summation over the discrete imaginary frequency, $S_\eta = T \sum_{i\omega_n} g(i\omega_n)$, where $g(i\omega_n)$ is a rational function, $\omega_n = 2n\pi T$ for bosons and $\omega_n = (2n + 1)\pi T$ for fermions and $n = 0, \pm 1, \pm 2, \dots$ is an integer (plays the role of a quantum number). By using Matsubara weighting function $h_\eta(z)$, which has simple poles exactly located at $z = i\omega_n$, then

$$S_\eta = \frac{T}{2\pi i} \oint g(z) h_\eta(z) dz, \quad (59)$$

where $\eta = \pm$ stands for the statistic sign for bosons and fermions, respectively. $h_\eta(z)$ can be chosen depending on which half plane the convergence is to be controlled,

$$h_\eta(z) = \begin{cases} \eta \frac{1+n_\eta(z)}{T}, \\ \eta \frac{n_\eta(z)}{T}, \end{cases} \quad (60)$$

where $n_\eta(z) = (1 + \eta e^{z/T})^{-1}$ is the single-particle distribution function.

The mesonic masses are conjectured to have contributions from Matsubara frequencies [71]. Furthermore, at high temperatures ($\geq T_c$), the behavior of the thermodynamics quantities, including the quark susceptibilities, besides the masses is affected by the interplay between the lowest Matsubara frequency and the Polyakov loop-correction [72]. We apply normalization for the different mesonic sectors with respect to the lowest Matsubara frequency [73] in order to characterize the dissolving temperature of the mesonic bound states. It is found that the different mesonic states have different dissolving temperatures. This would mean that the different mesonic states have different T_c 's, at which the bound mesons begin to dissolve into quarks. Therefore, the masses should not be different at $T > T_c$. To a large extend, their thermal and dense dependence should be removed, so that the remaining effects are defined by the free energy [71], i.e. the masses of *free* mesons are defined by m_i .

That the masses of almost all mesonic states become independent on T , i.e. constructing kind of a universal line. This would be seen as a signature for meson dissociation into quarks. It is a deconfinement phase-transition, where the quarks behave almost freely. In other words, the characteristic temperature should not be universal, as well. So far, we conclude that the universal T_c characterizing the QCD phase boundary is indeed an approximative average (over various bound states).

A. Critical Temperatures and Critical Chemical Potentials

In left-hand panel of Fig. 11, it is obvious that each scalar/pseudoscalar meson normalized to the lowest Matsubara frequency begins to dissolve into its quark constituents, individually. At very high temperatures, we expect a universal line independent on temperatures, where many bound particles dissolve, entirely. For example, κ , K , a_0 , η , η' , f_0 , σ and π dissolve, slowly. The right-hand panel shows the same behavior but corresponding to vector/axial-vector mesons, where ρ , ω , a_1 , f_1 dissolve, rapidly, while f_1^* is the last bound state, which seems to survive the typical T_c . In Tab. IV, different meson states are listed corresponding to their dissolving temperatures.

In Fig. 16, the top panels show the in-medium effects of the chemical potential (density) on the masses of mesonic states normalized to the lowest Matsubara frequency, at a fixed temperature lower than the typical T_c . It is obvious that increasing μ also brings the masses very close to a universal value, i.e., free energy. The bottom panels show the same but at a fixed temperature higher than the typical T_c . Here, increasing μ seems to bring the masses very close to a universal value in faster and easier way.

Finally, it is apparent that the temperature (an essential quantity in the lowest Matsubara frequency) should be corrected/weighted in order for the matrix model to reproduce the mean field results, correctly [72].

VI. MESON MASSES IN LARGE- N_c LIMIT

When replacing the QCD gauge symmetry $SU(3)$ by $SU(N_c)$, where $N_c \gg 3$ is the number of colors, we obtain a simpler QCD-theory. In other words, such a large- N_c limit offers an effective approach to study the QCD [74]. The relevant quantities can be given in N_c^{-n} -series, so that large- N_c dominant can be separated from suppressed terms. In doing this

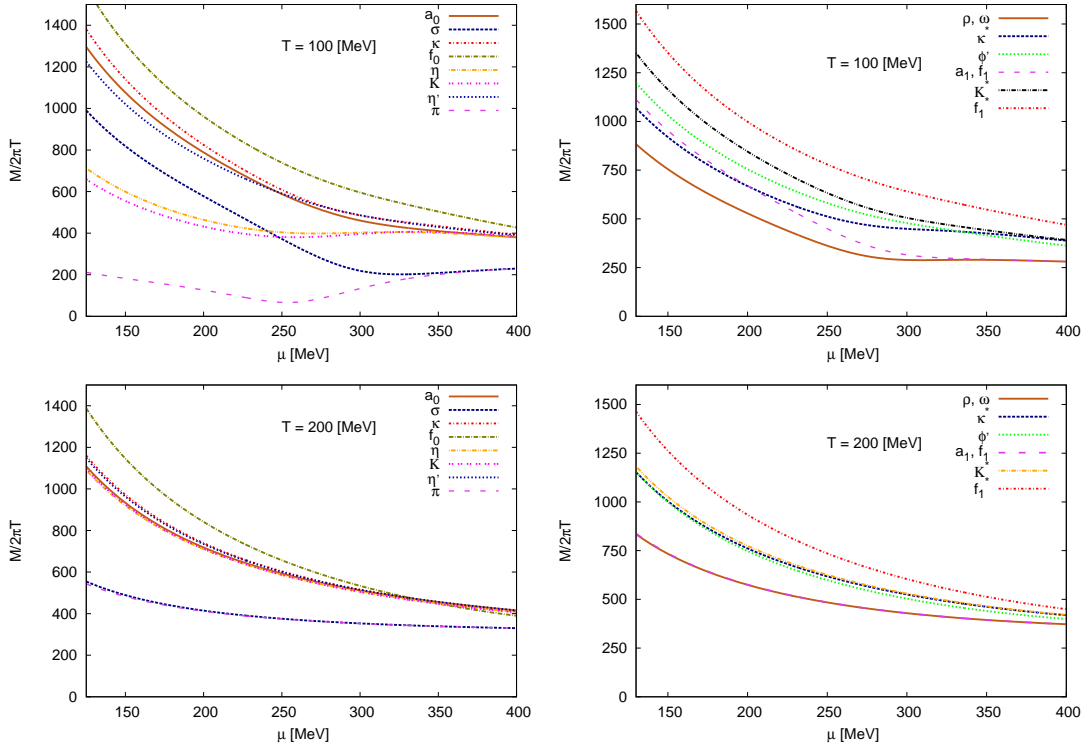


Fig. 16: (Color online) Left-hand panel shows scalar/pseudoscalar mesons at $T < 100$ MeV and at $T > 200$ MeV. The right-hand panel presents to vector/axial-vector mesons.

and in order to guarantee consistent large- N_c approach, the QCD coupling g_{QCD} must be scaled [70]; $g_{QCD} N_c \rightarrow \text{finite}$, if $N_c \rightarrow \infty$. Accordingly, it was concluded in Ref. [70] that the meson masses scale with N_c while the interaction scales with $N_c^{-(k-2)/2}$. The decay amplitudes are suppressed as $1/\sqrt{N_c}$ [70]. In this limit, the meson masses will be stable and non-interacting. At finite T , a non-interacting gas of mesons is realized for $N_c \gg 3$.

In defining the quarkyonic phase [75] which is conjectured to separate hadronic from partonic phases in the T - μ phase diagram, the large- N_c approach has been implemented [76]. Accordingly, the limits for the chiral models should be corrected for low-energy hadrons (having densities close to that of the nuclear matter) [75]. At very low temperatures, this should agree with the Walecka limit [77]. The properties of nuclear matter and chiral phase-transition have been investigated in the large- N_c limit [74, 75]. There is only one case in which nuclear matter does not disappear by increasing N_c . This is the naive quarkonium assigned to the lightest scalar resonance [78]. The low-energy hadrons (light scalar states below 1 GeV) do not formulate quarkonium states, predominantly. On the other hand, the resulting nucleon-nucleon attraction in the scalar channels is not strong enough to bind nuclei [74, 75].

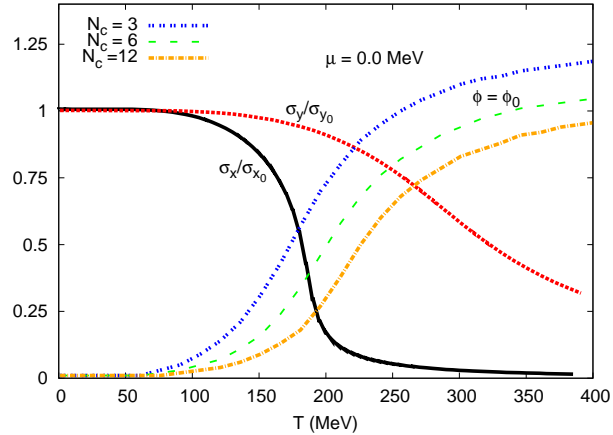


Fig. 17: (Color online) normalized chiral condensates σ_x and σ_y (solid and dotted curves, respectively) and the expectation values of the Polyakov loop, ϕ and ϕ^* , dotted curve ($N_c = 3$), dashed curve ($N_c = 6$), dotted dash ($N_c = 12$) respectively, are given as function of the temperature at vanishing chemical potential.

	$N_c = 3$	$N_c = 6$	$N_c = 12$
T_c^l	181	189	195
T_c^s	225	245	270

Tab. VII: Dependence of the critical temperatures in MeV for light T_c^l and strange-quark T_c^s on N_c .

In order to study the behavior of the meson masses with varying N_c , we start with calculating the PLSM normalized chiral-condensates, σ_x and σ_y , and the Polyakov-loop fields, ϕ and ϕ^* , at finite temperatures and vanishing chemical potential, Fig. VI. We find that ϕ and ϕ^* are good indicators for the deconfinement phase-transition. Both order parameters possess information about the confining glue-sector to the effective chiral-model; LSM. From the quarks-antiquarks potential, Eqs. (18), (19) and (30), it is obvious that the Polyakov-loop expectation values vary with N_c . We expect that the deconfinement phase-transition moves to higher critical-temperatures with increasing N_c and $T_c \rightarrow \infty$ when $N_c \rightarrow \infty$. Tab. VII summarizes T_c for light and strange quarks at different N_c .

Fig. 18 shows the scalar meson sectors at different N_c as function of T at $\mu = 0$ and $N_c = 3$ (solid curves), $N_c = 6$ (dotted curves), $N_c = 12$ (dash-dotted curves) and $N_c \rightarrow \infty$ (dashed curves). The masses of all mesons are not influenced when varying N_c . It seems that the mesons are stable and noninteracting, especially at densities close to that of the

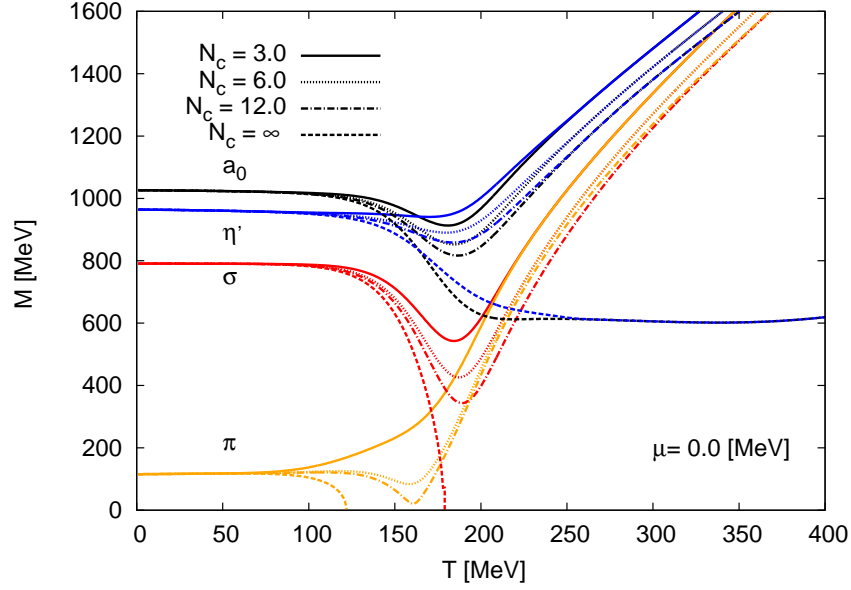


Fig. 18: (Color online) The scalar meson masses are given as function of T at $\mu = 0$ and $N_c = 3$ (solid curves), $N_c = 6$ (dotted curves), $N_c = 12$ (dash-dotted curves) and $N_c \rightarrow \infty$ (dashed curves).

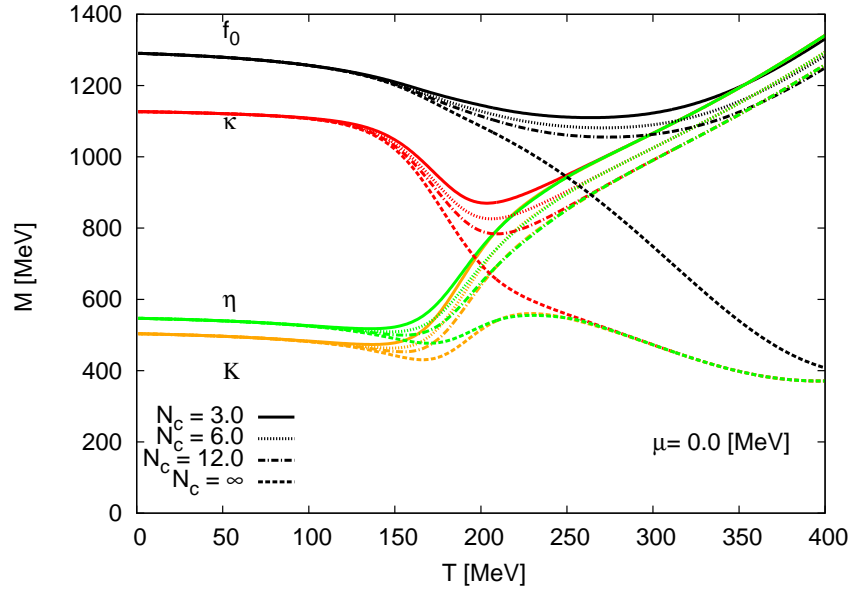


Fig. 19: (Color online) The same as in Fig. 18 but for pseudoscalar meson masses.

nuclear matter. At very low temperatures, the results seem to agree with a Walecka-like model [77]. The meson channels can be divided into three regions; one at low T , one around T_c and one at very high T .

- The first region is established where the strong force between quarks should be dominant and the mass degeneration appears despite of the variation of N_c . This can be interpreted as the effect of the vacuum contributions on the chiral symmetry-restoration.

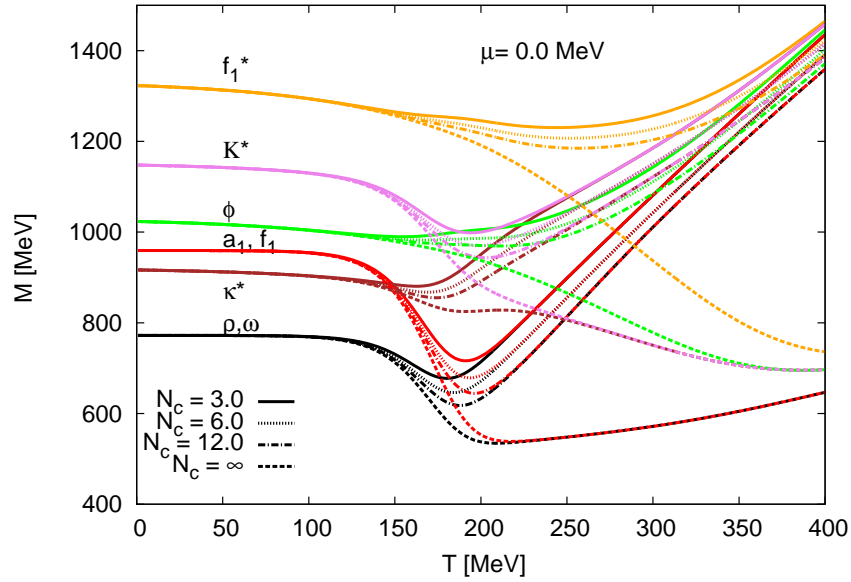


Fig. 20: (Color online) The same as in Fig. 18 but for axial and axialvector meson masses.

- The second region takes place due to fluctuations in the variation of colors N_c relating to the deconfinement phase-transition at T_c .
- In the last region, the bosonic thermal-contributions are dominant and the mass gap between mesons seems to disappear. The mesonic states degenerate at large N_c .

In the large- N_c limit, the meson masses are stable and noninteracting at low T . They keep the mass gap between the different meson channels. At high T , this gap disappears and the masses become T -independent. Except π and σ , the other scalar meson masses are T -independent at large N_c and high T . For the pseudoscalar meson masses, Fig. 19, the large N_c limit unifies the T -dependence of all states in a universal bundle. The same is also observed for axial and axialvector meson masses in the large- N_c limit, Fig. 20.

VII. CONCLUSIONS

There are various approaches implementing theoretical descriptions of the hadron masses in thermal and hadronic dense medium [21–23, 40, 41]. The NJL (or PNJL) studies the thermal spectrum of eight mesons; four scalars and four pseudoscalars at vanishing and finite chemical potential [24, 25]. Previous works using LSM (or PQM) focused on the study of (pseudo)-scalar mesons at finite temperature but vanishing density (chemical potential) [21–23, 40, 41] and described the vacuum phenomenology of some states in scalar and vector

meson nonets, besides the comparison with the experimental measurements for the decay width and the scattering length [31–36].

In the present work, a systematic study using the chiral symmetric linear σ -model is introduced. Scalar, pseudoscalar, vector, and axial-vector fields are included. The representation of all these four categories in dependence on the temperature and the baryon chemical density is taken into consideration. This allows us to define the characteristics of the chiral phase-structure for all these mesonic states, i.e., in thermal and hadronic dense medium and determine the critical temperature and density at which each mesonic state breaks into its free quarks.

At vanishing temperature, the scalar, pseudoscalar, vector and axial-vector meson nonets calculated in the present work are confronted to the experimental measurements reported by PDG [28]. Also, we compare the results with the lattice QCD calculations [26, 27] for pseudoscalar and vector mesons. The scalar and pseudoscalar spectrum calculated from PNJL [24, 25] is compared with the present work. We first want to highlight that the uncertainties are deduced from the fitting for the parameters used in calculating the equation of states and other thermodynamics quantities. The fitting requires information from the experimental data for axial/axialvector and scale/pseudoscalar states. Thus, we conclude that the results are very precise for some of the lightest hadron resonances. The effects of the chiral condensate and the deconfinement phase-transition would play an important role in charactering the chiral phase-structure of many hadrons and therefore, explain the differences seen in the heavy states. The PNJL model is limited to study (pseudo)-scalar meson states. Only pseudoscalar and vector meson masses are available in the lattice QCD calculations (HotQCD Collaboration) [26] and (PACS-CS Collaboration) [27]. Relative to these two approaches, it can be concluded that the present work reproduces well the mesonic spectrum.

In order to investigate the influence of the Polyakov loop-potential on the chiral symmetry-restoration, the present results are compared with PLSM. PLSM mainly describes the chiral condensates in non-strange σ_x and strange σ_y condensate in addition of the deconfinement phase-transition, ϕ and ϕ^* , in temperature and density (chemical potential) dependence. This allows the estimation of the spectrum of some mesonic states in SU(3) as a result of the chiral phase-structure of scalar/pseudoscalar and axial/axialvector states at various densities and temperatures. First, we compare the critical temperatures calculated from the inflection points of the phase transition and the order parameters. We

found that the chiral phase-transition gets shifted to higher temperatures as a result of the inclusion of the Polyakov loop in LSM. In the mesonic masses, the thermal bosonic contributions decrease with increasing the temperature, while the fermionic contributions increases at high temperature. At low temperatures, the fermionic contributions are negligible. The early (related to low critical temperature and/or small chemical potential) melting of the strange condensate σ_y relative to the non-strange one can be interpreted due to the mass degeneration at larger values of temperature and/or chemical potential. In the phase, where the symmetry is explicitly broken in PLSM, the meson masses generated by PLSM have a good agreement with the experimental results.

We have illustrated that the PLSM can be used to check which mesonic states degenerate with (an)other one(s) and which states degenerate faster relative to the other ones, especially near the Fermi surface. The limitation that all hadrons should melt at a universal critical temperature (QCD phase boundary) can be understood as an approximation. We conclude that each bound state would have a characteristic temperature and density (chemical potential) at which it dissolves to its free quarks. We plan to extend this study to include more mesonic states and characterize their thermal and dense evolution. Also, we want to introduce some low-lying baryonic states. Such a plan requires a basic modification of the Lagrangian. The normalization of various meson masses to the lowest Matsubara frequency removes all thermal dependence of the bound mesons and estimates the individual dissolving temperatures. It has been found that the various mesonic states have different dissolving temperatures and chemical potentials, i.e. they survive the *typically-averaged* QCD phase boundary, defined by the QCD critical temperatures with varying chemical potentials.

We have studied the thermal behavior of meson masses in the large- N_c limit. At low temperatures, we find that the meson masses are stable and noninteracting. with increasing temperature, they keep the mass gap between the different meson channels. At high T , this gap disappears and the masses become T -independent. The scalar meson masses are T -independent at large N_c and high T (except π and σ). For the pseudoscalar meson masses, the large N_c limit unifies the T -dependence of all states in a universal bundle. The same is also observed for axial and axialvector meson masses in the large- N_c limit.

Acknowledgements

This research has been supported by the World Laboratory for Cosmology And Particle Physics (WLCAPP), Cairo-Egypt, <http://wlcapp.net/>. AT is very grateful to Dirk H. Rischke and Denis Parganlija for the fruitful discussions the careful reviewing of the script.

-
- [1] M. Gell-Mann and M. Levy, *Nuovo Cim.* **16**, 705 (1960).
 - [2] C. Vafa and E. Witten, *Nucl. Phys.* **B 234**, 173 (1984);
L. Giusti and S. Necco, *JHEP* **0704**, 090 (2007).
 - [3] C. Amsler and N. A. Tornqvist, *Phys. Rept.* **389**, 61 (2004).
 - [4] E. Klempt and A. Zaitsev, *Phys. Rept.* **454**, 1 (2007).
 - [5] A. M. Polyakov, *Phys. Lett. B* **72**, 477 (1978).
 - [6] L. Susskind, *Phys. Rev. D* **20**, 2610 (1979).
 - [7] B. Svetitsky and L. G. Yaffe, *Nucl. Phys. B* **210**, 423 (1982).
 - [8] B. Svetitsky, *Phys. Rept.* **132**, 1 (1986).
 - [9] J. T. Lenaghan and D. H. Rischke, *J. Phys, G* **26**, 431-450 (2000).
 - [10] N. Petropoulos, *J. Phys, G* **25**, 2225-2241 (1999).
 - [11] M. Levy, *Nuovo Cim.***52**, 23 (1967).
 - [12] B. Hu, *Phys. Rev. D* **9**, 1825-1834 (1974).
 - [13] J. Schechter and M. Singer, *Phys. Rev. D* **12**, 2781 (1975).
 - [14] H. B. Geddes, *Phys. Rev. D* **21**, 278 (1980).
 - [15] B.-J. Schaefer and M. Wagner, *Nucl. Phys.* **62**, 381 (2009).
 - [16] H. Mao, J. Jin and M. Huang, *J. Phys. G* **37**, 035001 (2010).
 - [17] J. Wambach, B.-J. Schaefer and M. Wagner, *Acta Phys. Polon. Supp.* **3**, 691-700 (2010).
 - [18] A. Tawfik, N. Magdy and A. Diab, *Phys. Rev. C* **89**, 055210 (2014).
 - [19] B.-J. Schaefer, M. Wagner, and J. Wambach, **PoS CPOD**, 017 (2009).
 - [20] B.-J. Schaefer and M. Wagner, *Phys. Rev. D* **85**, 034027 (2012).
 - [21] B.-J. Schaefer and M. Wagner, *Phys. Rev. D* **79**, 014018 (2009).
 - [22] U. S. Gupta and V. K. Tiwari, *Phys. Rev. D* **81**, 054019 (2010).
 - [23] V. K. Tiwari, *Phys. Rev. D* **88**, 074017 (2013).
 - [24] T. Xia, L. He and P. Zhuang, *Phys. Rev. D* **88**, 056013 (2013).

- [25] P. Costa, M. C. Ruivo, C. A. de Sousa, H. Hansen and W. M. Alberico, Phys. Rev. D **79**, 116003 (2009);
P. Costa, M. C. Ruivo, C. A. de Sousa and Yu. L. Kalinovsky, Phys. Rev. D **71**, 116002 (2005);
P. Costa, M. C. Ruivo, C. A. de Sousa and Yu. L. Kalinovsky, Phys. Rev. D **70**, 116013 (2004).
- [26] A. Bazavov, *et al.* (HotQCD Collaboration), Phys. Rev. D **85**, 054503 (2012).
- [27] S. Aoki, *et al.* (PACS-CS Collaboration), Phys. Rev. D **81**, 074503 (2010).
- [28] J. Beringer *et al.* (Particle Data Group), Phys. Rev. D **86**, 010001 (2012).
- [29] B.-J. Schaefer, M. Wagner and J. Wambach, Phys. Rev. D **81**, 074013 (2010).
- [30] R. Stiele, E. S. Fraga and J. Schaffner-Bielich, Phys. Lett. B **729**, 72-78 (2014).
- [31] D. Parganlija, F. Giacosa and D. H. Rischke, Phys. Rev. D **82**, 054024 (2010).
- [32] S. Gallas, F. Giacosa and D. H. Rischke, Phys. Rev. D **82**, 014004 (2010).
- [33] D. Parganlija, P. Kovacs, G. Wolf, F. Giacosa and D. H. Rischke, Phys. Rev. D **87**, 014011 (2013).
- [34] P. Kovacs, G. Wolf, F. Giacosa and D. Parganlija, Europhys. J. **13**, 02006 (2011).
- [35] D. Parganlija, P. Kovacs, G. Wolf, F. Giacosa and D. H. Rischke, AIP Conf. Proc. **1520**, 226-231 (2013).
- [36] S. Gallas, F. Giacosa and D. H. Rischke, Phys. Rev. D **82**, 014004 (2010).
- [37] B.-J. Schaefer, J. M. Pawłowski and J. Wambach, Phys. Rev. D **76**, 074023 (2007).
- [38] L. M. Haas, R. Stiele, J. Braun, J. M. Pawłowski and J. Schaffner-Bielich, Phys. Rev. D **87**, 076004 (2013).
- [39] A. Tawfik and N. Magdy, " *On $SU(3)$ models for chiral phase transition*", in Progress.
- [40] S. Struber and D. H. Rischke, Phys. Rev. D **77**, 085004 (2008).
- [41] J. T. Lenaghan, D. H. Rischke and J. Schaffner-Bielich, Phys. Rev. D **62**, 085008 (2000).
- [42] D. Parganlija, F. Giacosa and D. H. Rischke, AIP Conf. Proc. **1030**, 160-164 (2008).
- [43] D. Parganlija, F. Giacosa and D. H. Rischke, PoS CONFINEMENT **8**, 070 (2008).
- [44] S. Gasiorowicz and D. A. Geffen, Rev. Mod. Phys. **41**, 531 (1969).
- [45] P. Ko and S. Rudaz, Phys. Rev. D **50**, 6877 (1994).
- [46] J. Boguta, Phys. Lett. B **120**, 34 (1983);
O. Kaymakçalan and J. Schechter, Phys. Rev. D **31**, 1109 (1985);
Robert D. Pisarski, *Applications of chiral symmetry*, Talk at workshop on Finite Temperature QCD and Quark - Gluon Transport Theory, 18-26 Apr 1994. Wuhan, China (1994).

- [47] P. Kovacs and G. Wolf, *Acta Phys. Polon. Supp.* **6**, 853-858 (2013).
- [48] C. Rosenzweig, J. Schechter and C. G. Trahern, *Phys. Rev. D* **21**, 3388 (1980).
- [49] A. H. Fariborz, R. Jora and J. Schechter, *Phys. Rev. D* **77**, 094004 (2008).
- [50] S. Weinberg, *Phys. Rev. D* **11**, 3583 (1975).
- [51] Dirk H. Rischke and Denis Parganlija, private communication
- [52] V. I. Borodulin, R. N. Rogalev and S. R. Slabospitsky, *CORE: COmpendium of RElations: Version 2.1*, hep-ph/9507456
- [53] P. Kovacs and Z. Szep, *Phys. Rev. D* **75**, 025015 (2007).
- [54] K. Fukushima, *Phys. Lett. B* **591**, 277 (2004).
- [55] C. Ratti, M. A. Thaler and W. Weise, *Phys. Rev. D* **73**, 014019 (2007).
- [56] S. Roessner, C. Ratti and W. Weise, *Phys. Rev. D* **75**, 034007 (2007).
- [57] K. Fukushima, *Phys. Rev. D* **77**, 114028 (2008).
- [58] B.-J. Schaefer, J. M. Pawłowski and J. Wambach, *Phys. Rev. D* **76**, 074023 (2007).
- [59] B.-J. Schaefer and J. Wambach, *Phys. Rev. D* **75**, 085015 (2007).
- [60] Denis Parganlija, Peter Kovacs, Gyrgy Wolf, Francesco Giacosa, Dirk H. Rischke, PoS ConfinementX, 117 (2012).
- [61] O. Scavenius, A. Mocsy, I. N. Mishustin and D. H. Rischke, *Phys. Rev. C* **64**, 045202 (2001).
- [62] J. I. Kapusta and C. Gale, *"Finite-temperature field theory: Principles and applications"*, (Cambridge University Press, Cambridge, 2006).
- [63] A. Bazavov (HotQCD Collaboration) **PoS LATTICE2011**, 182 (2011).
- [64] A. Tawfik, *Phys. Rev. D* **71**, 054502 (2005).
- [65] E. Laermann, *Nucl. Phys. A* **702**, 134-139 (2002).
- [66] J. Kapusta, *Finite-Temperature Field Theory*, (Cambridge University Press, Cambridge, 1989).
- [67] Mathias Wagner, *"The Chiral and Deconfinement Phase Transitions in Strongly Interacting Matter"*, (Thesis, Darmstadt, 2008).
- [68] E. Witten, *Nucl. Phys. B* **156**, 269 (1979);
G. Veneziano, *Nucl. Phys. B* **59**, 213 (1979).
- [69] V. Koch, *Int. J. Mod. Phys. E* **6**, 203 (1997).
- [70] A. Heinz, F. Giacosa and D. H. Rischke, *Phys. Rev. D* **85**, 056005 (2012).
- [71] W. Florkowski and B. L. Friman, *Z. Phys. A* **347**, 271 (1994).

- [72] K. Dusling, C. Ratti and I. Zahed, Phys. Rev. D **79**, 034027 (2009).
- [73] A. Tawfik, Soryushiron Kenkyu **114**, B48-B50 (2006).
- [74] G. 't Hooft, Nucl. Phys. **75**, 461 (1974); E. Witten, Nucl. Phys. B **160**, 57 (1979).
- [75] F. Giacosa, "*Nuclear Matter and Chiral Phase Transition at Large- N_c* ", 1106.0523 [hep-ph]
- [76] L. D. McLerran and R. D. Pisarski, Nucl. Phys. A **796**, 83 (2007).
Y. Hidaka, L. D. McLerran and R. D. Pisarski, Nucl. Phys. A **808**, 117, (2008).
- [77] J. D. Walecka, Annals Phys. **83**, 491 (1974).
B. D. Serot and J. D. Walecka, Adv. Nucl. Phys. **16**, 1 (1986).
B. D. Serot and J. D. Walecka, Int. J. Mod. Phys. E **6**, 515 (1997).
- [78] L. Bonanno and F. Giacosa, Nucl.Phys. A **859**, 49 (2011).